Fall 2017

Vulnerability Assessment of Critical Bridges in the Hampton Roads Region of Virginia to Storm Surge Flooding under Sea Level Rise

Luca Castrucci
Old Dominion University, lcast012@odu.edu

VULNERABILITY ASSESSMENT OF CRITICAL BRIDGES IN THE HAMPTON ROADS REGION OF VIRGINIA TO STORM SURGE FLOODING UNDER SEA LEVEL RISE

by

Luca Castrucci
B.S. May 2016, Old Dominion University

A Thesis Submitted to the Faculty of
Old Dominion University in Partial Fulfillment of the
Requirements for the Degree of

MASTER OF SCIENCE

CIVIL ENGINEERING

OLD DOMINION UNIVERSITY
December 2017

Approved by:

Navid Tahvildari (Director)

Ma Gangfeng (Member)

Mecit Cetin (Member)

ABSTRACT

VULNERABILITY ASSESSMENT OF CRITICAL BRIDGES IN THE HAMPTON ROADS REGION OF VIRGINIA TO STORM SURGE FLOODING UNDER SEA LEVEL RISE

Luca Castrucci
Old Dominion University, 2017
Director: Dr. Navid Tahvildari

In this thesis, a hydrodynamic model was developed to study the vulnerability of the transportation infrastructure in the Hampton Roads region of Virginia to storm surge flooding under sea level rise. The Hampton Roads region is the second most affected area by relative sea level rise in the United States. The hydrodynamic model was validated for tide prediction, and its performance in storm surge simulation was validated with data from Hurricane Irene (2011). The developed model was then applied to eight flood-prone bridges in the transportation network that connect the cities of Norfolk, Hampton, Virginia Beach, Chesapeake and Portsmouth; the extent, intensity, and duration of storm surge inundation under different sea level rise (SLR) scenarios was estimated. Furthermore, the difference between the results of the model and the simplistic "bathtub" approach in estimating flooding was highlighted.

This thesis is dedicated to my family and to my grandmother Maria Spadaro, who I miss so much.

ACKNOWLEDGMENTS

I extend many thanks to Dr. Mecit Cetin for his patience and help in successfully completing my thesis defense. For his tireless dedication to my research, my advisor Dr. Navid Tahvildari deserves special recognition. We started this study with very limited knowledge of hydrodynamic modeling, and despite the many problems faced, I was able to obtain good results counting only on myself and my advisor. Special thanks goes also to Dr. Ma Gangfeng for introducing me to Coastal Engineering.

This paragraph is dedicated to all the people that made a difference in my life, starting with my parents Rita and Roberto. Through my educational career, they never stopped supporting and believing in me. I am also immensely grateful for the infinite love that my grandparents gave me. A special dedication to my sister Chiara and my best friend Marco; having them close to me has always been a source of motivation for improving myself; without them I would have never become who I am today. Last but not least, I want to express my gratitude to the friends I met here at Old Dominion University and to the Calcagni family for everything they have done for me, in particular to Anne and Antonio.

TABLE OF CONTENTS

Page

LIST OF TABLES

LIST OF FIGURES

Figure Page

CHAPTER 1

INTRODUCTION

CO_2 emission in the atmosphere related to human activity is considered the main cause of climate change, which in this century will result in increased global average temperatures, precipitation, extreme weather events such as hurricanes, sea level, and extreme heat (EPA, 2009). Coastal environments are expected to be one of the ecosystems most severely impacted due to climate change effects on water level and weather events (Ashton et al., 2008; Bender et al., 2010; Harvey and Nicholas, 2008). Sea level rise combined with an increase in precipitation and extreme weather events is not only a potential danger for natural coastal environments, causing habitat destruction and a high level of erosion, but also for transportation infrastructure (CSIRO, 2007). Destructive consequences for manmade structures could include the flooding of tunnels, streets and urban areas within drainage basins as well as the washing out of bridges and roads along the shoreline. Oceanographers, coastal engineers and adaptation specialists use numerous hydrodynamic models to predict future flooding under sea level rise with or without considering a storm surge component. Some of the well-known models are: Delft3D (Vatvani et al., 2012), ADCIRC (Westerink et al., 2008), FVCOM (Yoon et al., 2014), MIKE (Sto. Domingo et al., 2010), and SLOSH (Murdukayeva et al., 2013). The alternative to hydrodynamic models is Geographical Information System (GIS) based models like HAZUS, developed and currently used by the U.S. Federal Emergency Management Agency (FEMA). GIS models exclusively focus on spatial analysis and estimate vulnerable areas by considering the land elevation with respect to the sea level rise scenario chosen. This method of vulnerability assessment is also known as the ‘bathtub approach’ and has been used in multiple previous studies (Kont et al., 2008; van De Sande et al., 2012; McInnes et al., 2013). The advantage of this approach is the

rapid identification of potential flooding hazards for a large area without requiring a long modeling process. However, in terms of accuracy, the lack of consideration for the flow dynamics process makes the GIS models over-estimate flooding with respect to hydrodynamic modeling (Seenath et al., 2015). The importance of reliable and easily accessible vulnerability studies on flooding driven by climate change is gaining more and more consideration for emergency coastal planning decisions (Bhaskaran et al., 2014).

Climate change impacts will differ according to the region considered. As an example, the U.S. Atlantic coast is affected by a higher than average sea level rise due to variations given by glacial isotactic adjustments and oceanographic processes (Sallenger et al., 2012). Considering sea level rise based on the local scale justifies the creation of a new term: relative sea level rise. Along the U.S. Atlantic coast and the rest of the United States of America, the most impacted areas by relative sea level can be identified as Florida, Louisiana and the entire region between Massachusetts and Virginia (Engelhart et al., 2011).

The Hampton Roads (Fig. 1) region in Virginia is a low-lying coastal area in the Southeast Chesapeake Bay. It is a metropolitan region located at the confluence of the James, Elizabeth, and Nansemond Rivers and is comprised of ten cities with a total population of 1.7 million. The Port of Virginia, located in Hampton Roads, is the second largest port on the East Coast. Norfolk, which also falls within the Hampton Roads area, is home to the largest naval base in the world (Kleinosky et al., 2007). The region has the second highest relative SLR in the U.S. (~7 mm/yr) behind New Orleans (Boon et al., 2010). Several factors including crustal warping, sediment compaction and groundwater withdrawal as well as the dynamics of the Gulf Stream contribute to this high rate of relative SLR. The transportation infrastructure in the Hampton Roads region is considerably susceptible to recurrent flooding due to the combined

effects of precipitation and high tides, and SLR has exacerbated flooding in the region. A recent study shows that the region is experiencing an accelerated rate of minor flooding, and the transportation infrastructure in the region is increasingly subject to disruptions due to flooding events (Ezer and Atkinson, 2014). The effect of SLR on the coastal region is dynamic and includes an increase in storm surge flooding, wetland migration, and shoreline erosion (Passeri et al., 2015). It has been shown that the response of storm surge to increased sea level is nonlinear (Atkinson et al., 2013), thus flooding estimates accounting for SLR may vary by location following a dynamic process. This is due to the complex physics of the interactions between storm surge, tides, waves, and the overland flow as well as their interactions with the natural and urbanized landscape.

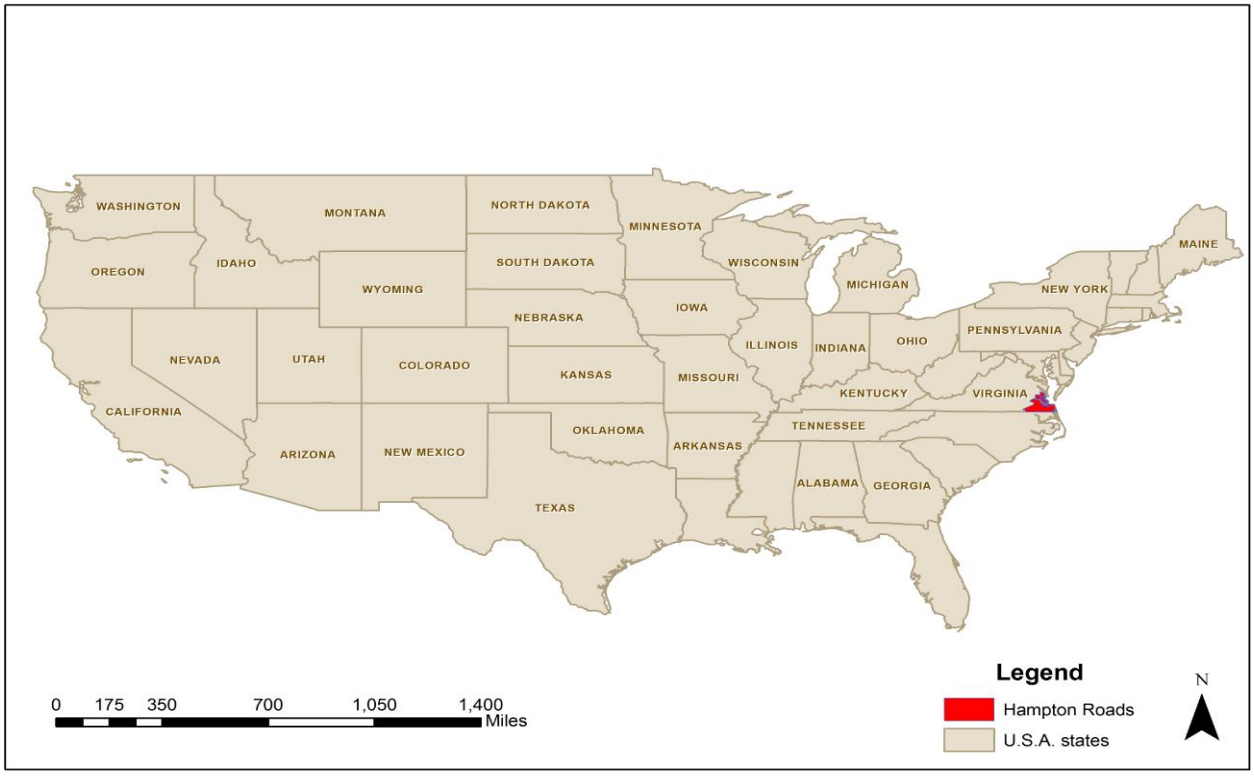

Fig. 1. Hampton Roads location in the United States of America.

In this context, the primary objective of my thesis will be to develop a hydrodynamic model to conduct a vulnerability analysis of flood-prone bridges in the Hampton Roads region of Virginia. The bridges will be selected based on ground elevation and traffic flow. This thesis expands the earlier investigation by Castrucci and Tahvildari (2017) which resulted in assessment of flood vulnerability in an area of Norfolk. The effects of various SLR projections on storm surge flooding are considered. Furthermore, results obtained under equal conditions from both the hydrodynamic model and "bathtub" approach will be compared and analyzed.

CHAPTER 2

LITERATURE REVIEW

Numerous reports were released to quantify the vulnerability of the Hampton Roads region to sea level rise. One of the first reports was released by the Chesapeake Bay Foundation in 2007 and focused attention on the climate change consequences within local ecosystems. It highlighted the importance of wetland preservation since wetlands act as a natural buffer against storms (Climate Change Report, 2007). The following year, the Commonwealth of Virginia commissioned a study about the consequences of climate change on cities for the entire state without giving much consideration to the coastal infrastructure system (Governor's Commission on Climate Change, 2008). In the last decades, the Virginia Institute of Marine Science (VIMS) has also been very active for hazard estimation in the Hampton Roads area. Using data from monitoring stations, Boon et al. (2010) estimated relative SLR and teased apart the effects of global sea level rise and local land subsidence. In addition, in collaboration with the Center for Coastal Resources Management at Old Dominion University, the Hampton Roads Planning District Commission, the City of Norfolk, the Accomack-Northampton Planning District Commission and Wetlands Watch, VIMS released a report with adaptation guidelines to prevent recurrent flooding in Tidewater and Eastern Shore Virginia localities (Recurrent Flooding study for Tidewater Virginia, 2013). Before being submitted to the Virginia General Assembly in 2013, the study was passed by the Senate (February 28, 2012) and the House of Delegates (February 24 2012).

Federal agencies, universities and research institutes also gave their attention to the Hampton Roads area, assessing climate change hazards through hydrodynamic and GIS models. For instance, Li et al. (2012) studied the impact of climate change on the Norfolk naval base by

coupling the hydrodynamic model ADCIRC with the third-generation wave model SWAN. The study showed how 80% of the naval base will flood during a 100-year storm on top of a relative sea level rise estimated at 2 meters. Applying several high-fidelity numerical models, in 2015 the US Army Corps of Engineers released a study with the goal to provide statistical nearshore waves and water level data for risk management analysis for the U.S. North Atlantic coast (Cialone et al., 2015). Loftis et al. (2016) used the subgrid-modeling approach (Neelz and Pender, 2007) to simulate the precipitation- and storm surge-driven flooding at NASA Langley Research Center. The approach allows for nesting high-resolution LiDAR elevation data in a lower resolution computational grid of the hydrodynamic model. They showed that flooding estimation improves by accounting for infiltration using land use data. The hydrodynamic model used in the study is the UnTRIM2 model (Casulli and Stelling, 2011). In a recent study, Sadler et al. (2017) estimated the most vulnerable transportation infrastructure in the Hampton Roads cities of Norfolk and Virginia Beach. Applying the "bathtub" approach, results suggested that under the intermediate scenario by 2100 around 10% of major roads in Virginia Beach and Norfolk were predicted to regularly flood due to tides reaching mean higher high water (2.1 m). This value increased to over 15% of major roads with a 99% tide (2.6 m) and to over 65% of major roads with the addition of a 100-year storm surge (4.5 m). The study uses the "bathtub" approach to add storm surge estimates to SLR projections. Consequently, earlier flooding studies have either used the "bathtub" approach (e.g. Sadler et al., 2017) or have used hydrodynamic models to focus on a small study area (Li et al., 2012; Loftis et al., 2016).

CHAPTER 3

METHODOLOGY

The hydrodynamic model of the region was developed based on the Delft3D model. Delft3D is a widely used three dimensional modeling suite that can simulate coastal, estuarine, and riverine processes. The model has recently been used for storm surge simulations (Vatvani et al., 2012; Hu et al., 2015). The hydrodynamic model solves the complex interactions between the flow and the landscape in the current and future sea level condition and provides high temporal and spatial resolution information on water surface elevation and flow velocity at points of interest. By comparing model output on water levels with high resolution topographic data obtained from a geographic information system (GIS), flooding extent, intensity, and duration for flood-prone bridges were determined. Hurricane Irene (2011) parameters were used to generate the storm surge. In addition to storm surge, the model accounts for tide effects on water level and considers three SLR scenarios: intermediate-low, intermediate-high, and extreme.

3.1 Study Areas

The critical flood-prone bridges were identified based on traffic load and elevation with respect to the vertical datum NAVD88. The traffic volume was evaluated based on the Annual Average Daily Traffic (AADT) data released by the Virginia Department of Transportation (VDOT) on June 15, 2017. The database contains information from 1985 to 2015. The elevation analysis was conducted using the most recent LiDAR data available for the state of Virginia. Developed between 2010 and 2016 by the consulting firm Dewberry, the LiDAR has a horizontal resolution of 0.76 meters and a vertical accuracy of 0.2 meters.

Sadler et al. (2017) classified roads with an elevation lower than 3 meters as vulnerable to flooding since this threshold represents a feasible high tide water surface elevation in 2100 (Sadler et al., 2017). For the assessment of bridge vulnerability to direct storm surge flooding, a higher threshold (3.5 meters) was chosen as a potential vulnerable elevation. According to these criteria, a group of eight different bridges were identified as at risk due to flooding. US 58 Brambleton Ave, located in the Hague neighborhood, James River and I-64 WB/EB bridges were later selected for further analysis that involved the development of dedicated hydrodynamic models. VA 337, US 58 Brambleton Ave provides access to Norfolk General Hospital, housing the region's only level 1 trauma center. The second and third bridges are both included in the local evacuation plan. Better flooding prediction provided by a dedicated hydrodynamic model will help decision makers provide advanced warnings and reroute traffic.

Table 1. List of the critical flood-prone bridges included in the thesis

Bridge Name	**Elevation Entry Road (m)**	**Elevation Exit Road (m)**	**AADT**	**Model #**
I-264 WB/EB	3.34	4.03	125000	2
I-64 WB/EB, US 17	6.17	3.50	91000	3
US 13 Military Highway	3.33	3.23	51000	2
VA 337, US 58 Brambleton Ave	1.3	2.29	37000	3
VA 337 Hampton Blvd	1.93	2.17	36000	2
US 60 Shore Dr	3.26	3.38	35000	2
US 460 Granby St	2.37	2.49	31000	2
James River Bridge	1.63	3.10	30000	3

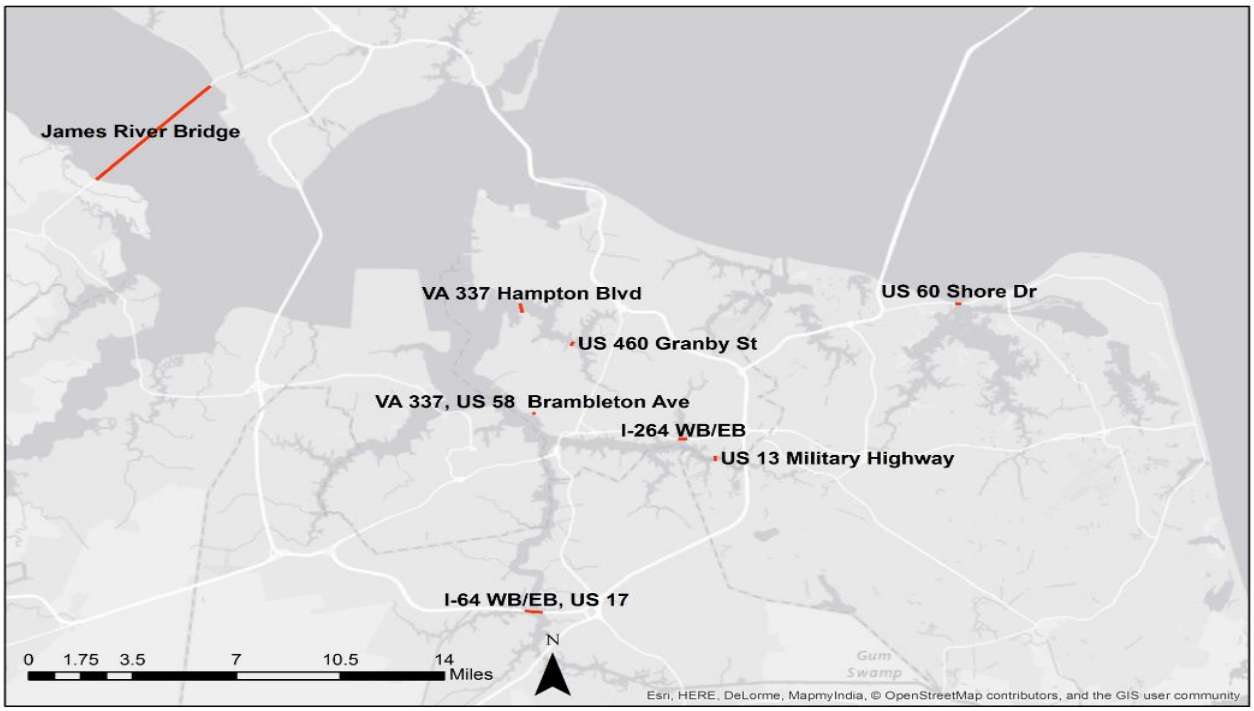

Fig. 2. Location of the critical flood-prone bridges included in the thesis.

3.2 Delft3D Model Set up

Delft3D–FLOW is a module that can simulate non-steady flow processes generated by tidal and meteorological forcing solving one-, two- and three-dimensional time-dependent, non-linear differential equations related to the free-surface flow problems on a structured orthogonal grid to cover a coastal area with complicated geometry. The model can estimate a wide variety of flow variables, namely velocity, pressure, and water surface elevation over the computational grid. The governing three-dimensional equations describing the water surface can be derived from the Navier-Stokes equations, and they account for the physical principle of conservation of volume, mass and momentum:

$$\frac{\partial u}{\partial t}+u\frac{\partial u}{\partial x}+v\frac{\partial u}{\partial y}+\frac{\omega}{(d+\varsigma)}\frac{\partial u}{\partial \sigma}-fv=-\frac{1}{\rho}P_u+F_u+\frac{1}{(d+\varsigma)^2}\frac{\partial}{\partial \sigma}\left(v_v\frac{\partial u}{\partial \sigma}\right) \quad (1)$$

$$\frac{\partial v}{\partial t}+u\frac{\partial v}{\partial x}+v\frac{\partial v}{\partial y}+\frac{\omega}{(d+\zeta)}\frac{\partial v}{\partial \sigma}-fu=-\frac{1}{\rho}P_v+F_v+\frac{1}{(d+\zeta)^2}\frac{\partial}{\partial \sigma}\left(v_v\frac{\partial v}{\partial \sigma}\right) \quad (2)$$

$$\frac{\partial \omega}{\partial \sigma}=-\frac{\partial \zeta}{\partial t}-\frac{\partial[(d+\zeta)\mathrm{u}]}{\partial x}-\frac{\partial[(d+\zeta)\mathrm{v}]}{\partial y}+H(q_{in}-q_{out})+P-E \quad (3)$$

$$\frac{\partial \zeta}{\partial t}+\frac{\partial\left[(d+\zeta)\int_{-1}^{0}\mathrm{u}\,d\sigma'\right]}{\partial x}-\frac{\partial\left[(d+\zeta)\int_{-1}^{0}\mathrm{v}\,d\sigma'\right]}{\partial y}=H(q_{in}-q_{out})+P-E \quad (4)$$

The three above equations describe the water level in shallow water conditions, assuming the vertical acceleration is smaller than the horizontal acceleration; thus, the vertical momentum equation is reduced to the hydrostatic pressure relation. Equations (1), (2) and (3) are momentum equations, whereas the (depth-integrated) continuity equation is described in (4). u(x,y,σ,t,), v(x,y,σ,t) and ω(x,y,σ,t) are the velocity components in the horizontal x, y and vertical σ-directions, respectively; ς(x,y) is the water level above a reference plane; d(x,y) is the depth below water level; H(x,y)=d(x,y)+ ς(x,y) is the total water depth, t is the time; f is the Coriolis parameter; g is the gravitational acceleration and v_v is the vertical eddy viscosity coefficient. Furthermore, in q_{in} and out q_{out} are the local sources and sinks of water per unit of volume; P represents precipitation and E the evaporation. The horizontal pressure terms are expressed with the term P_u and P_v and the horizontal viscosity terms F_u and F_v.

3.2.1 Grid Generation

The grid size was selected such that the results were obtained at high spatial resolution while keeping the computational time reasonable. It is noted that in a domain with a variety of grid sizes, the simulation time step is governed by the smallest cell. Therefore, an efficient way to run the simulations using structured grids is to define multiple models with different domain extents that have nearly uniform grid cell sizes. In this approach, known as model nesting, the model with a lower resolution and a larger domain provides the boundary condition for a smaller

nested model with a domain within the larger grid. It is noted that to produce high resolution output, meteorological forcing and boundary conditions must be provided to the model at high resolutions. In order to have a compromise between computational time and input/output resolution, the model was developed in three nested levels. The grid for the first level of nesting covers the largest domain and has the lowest resolution (Fig. 3). This grid is equidistant such that the distance between the center of each cell is the same. The cell size in this grid is 125×200 m^2. Upon validation with the data, the output of Model 1 along with the data on James River discharge will serve as the boundary conditions for the model in the second level of nesting. The grid in this model covers a smaller domain within the first grid (Fig. 4). It has a higher resolution with the cell size of around 30 ~ 90 × 30 ~ 90 m^2. Once the performance of the second model is validated, its output will be used as the boundary conditions for a third level nested model that utilizes a high-resolution grid built around the critical spots, highlighted in red boundaries in Fig. 4. The grid resolution in the third level nested model is 2.5-3.5 × 2.5-3.5 m^2 and enables development of high-resolution street-level flood maps. The third level of nesting was develop only for US 58 Brambleton Ave, I-64 WB/EB and VA 337, US 58 Brambleton Ave bridges, while the high resolution street-level flood maps for the other critical spots were developed refining to 9 ~ 10 × 9 ~ 10 m^2 the selected area of the second level of nesting. From now on, the models at the first, the second, and the third level of nesting will be referred as Models 1, 2, and 3, respectively.

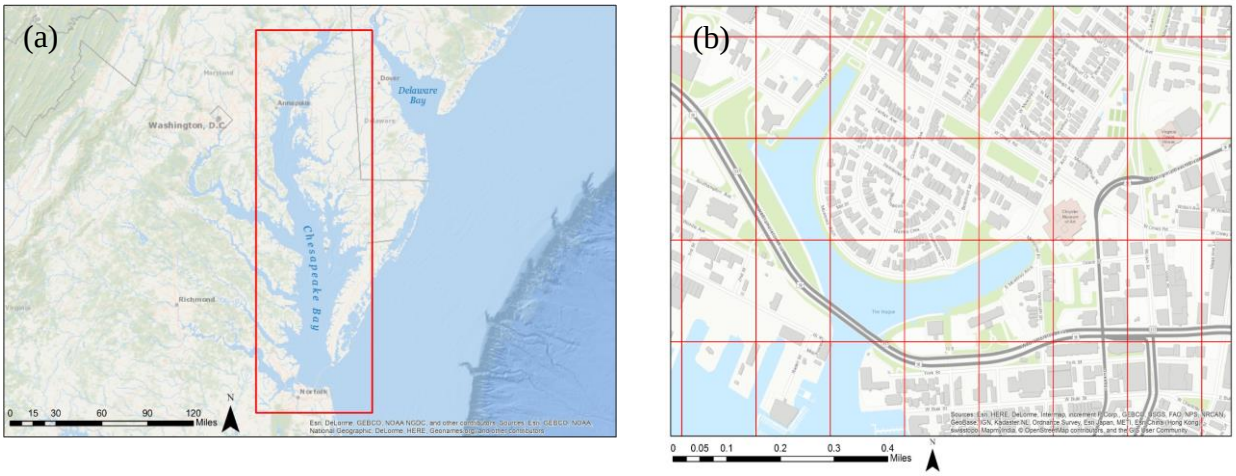

Fig. 3. (a) Delft3D model domain and (b) computational grid view of the Model 1.

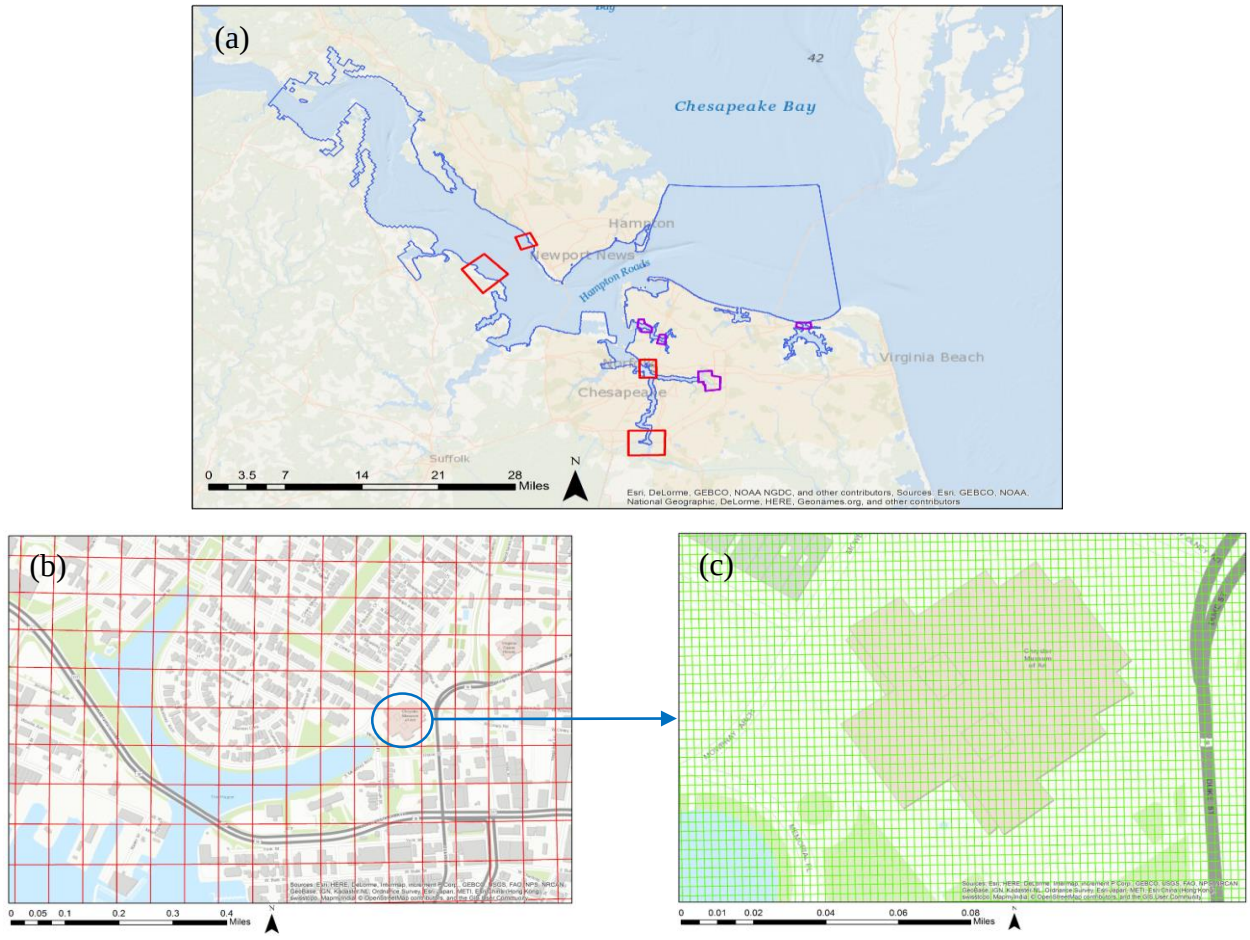

Fig. 4. (a) Delft3D model domain in blue for Model 2, purple for refine area of Model 2 and in red for Model 3. (b) computational grid view of Model 2. (c) computational grid view of the Model 3.

3.2.2 Boundary Conditions

The hydrodynamic storm surge model requires on topographic, bathymetric, tidal, wind profile, and river discharge data to perform the simulation.

3.2.2.1 Topographic and Bathymetric Data

The accuracy of the predictions of hydrodynamic models depends on the resolution of the available data (Sebastian et al., 2014). The high resolution LiDAR Virginia topographic data developed by Dewberry was used for Model 3. In Models 1 and 2, which have larger domains, we used the freely available highest resolution bathymetric and topographic data from National Oceanic and Atmospheric Administration (NOAA). Table 2 summarizes the sources of the topographic/bathymetric data used in the study as well as the spatial resolution of each dataset. The elevation data from different sources did not have the same datum and coordinate system and as such, they were converted to a common coordinate system and vertical datum. While the bathymetric and topographic had the same resolution in Models 1 and 2, their horizontal resolution differed in Model 3 (topography: 0.76 m, bathymetry: 10 m). Therefore, it was necessary to adapt and merge the datasets using ArcGIS prior to adequately formatting the data for the Delft3D model using Delft3D-QUICKIN triangular interpolation.

Table 2. The bathymetric and topographic data sources, resolution, and nested model level

Data	Source	Horizontal Resolution	Vertical Resolution	Model
Topography	NOAA – Coastal Relief Model	90 meters	1 meters	1
Topography	NOAA – Virginia Beach Raster	10 meters	0.3 meters	2
Topography	USGS – Hampton Roads LiDAR	0.76 meters	0.2 meters	3
Bathymetry	NOAA – Coastal Relief	90 meters	1/10 of a meter	1
Bathymetry	NOAA – Virginia Beach Raster	10 meters	0.3 meters	2 and 3

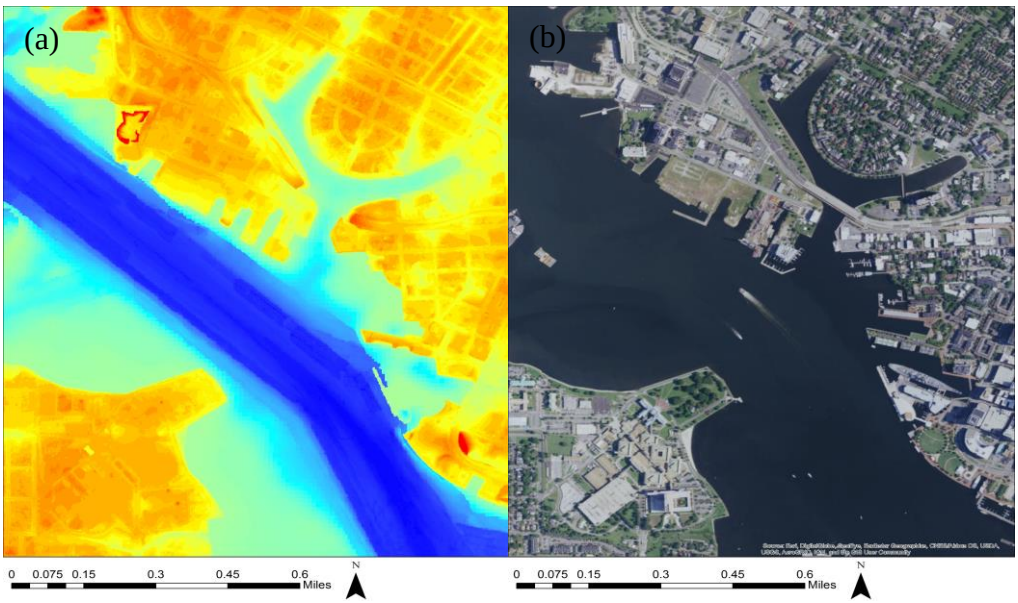

Fig. 5. Comparison between the (a) topography/bathymetry used for Model 3 and (b) a real view of the Hague neighborhood in Norfolk, VA.

3.2.2.2 Tides

High tides significantly contribute to flooding and as such, a storm surge model should accurately account for tides. The Delft3D model is forced by the tidal elevation and phase at the open boundaries of Model 1 with nine primary tidal constituents (M2, S2, N2, K2, K1, O1, P1,

Q1 and M4). The amplitudes and the phases of these harmonics were interpolated using the values from the TPXO global tide model (Egbert et al., 2002). The tide model has a 1/30° resolution at the U.S. East Coast. Using Matlab, the tidal information was extracted at the Model 1 boundary; the location near the coastline helped Delft3D to adequately reproduce the tidal propagation in shallow water. This allowed for compensation of the relatively low topography and bathymetry resolution provided by NOAA-Coastal Relief Model.

3.2.2.3 Wind Profile

The most important boundary condition in storm surge simulation is the hurricane's wind and pressure fields. According to the data from the NOAA tide gauge at Sewells Point, VA, Hurricane Irene (2011) together with Sandy (2012) and Isabel (2003) caused the largest storm surge among hurricanes that have affected the Hampton Roads region in the past decade. Due to the low resolution of real measurements for wind and pressure provided by satellites, the hurricane profile was created using the Holland et al. (2010) model to obtain reliable storm surge estimates. The Holland model generates the wind profile using the maximum wind velocity, minimum pressure, and storm diameter (Holland et al., 2010). The storm path, maximum wind velocity and minimum pressure were provided in the Hurricane Irene best track data released by the NOAA National Hurricane Center, while the storm diameter was estimated according to the Gross model (Gross et al., 2004). The output values from the Holland model were later inserted in a meteo grid which, shaped as a spider web (Fig. 6), can host variable grid sizes that increase resolution as they approach the center of the network. Since the dimension of Hurricane Irene changed multiple times over its path and the storm dimension varied with maximum velocity and central pressure, it was necessary to create a spider web domain large enough to accommodate

such changes. The main characteristic of the spider web domain is related to its non-stationary position, which during the simulation changes according to the hurricane path. Delft3D estimates the wind and pressure forces acting on water level through the interpolation between the spider web and hydrodynamic domains. The computed wind profile was used to validate model performance to estimate the historic storm surge levels as well as predict storm surge flooding due to Irene-like storms under future sea level conditions.

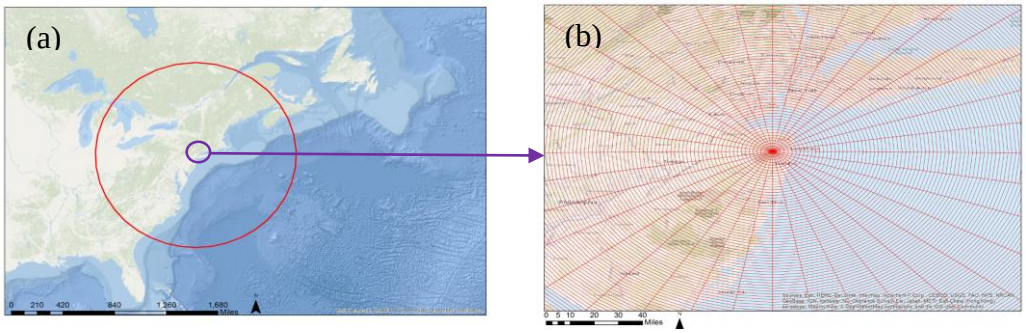

Fig. 6. (a) The extent of the spiderweb domain (red) for atmospheric forcing and (b) a view of the spiderweb computational grid at its center.

3.2.2.4 River Discharge

The discharge of the James River is used as a boundary condition in the western open boundary of Model 2. The River discharge is recorded every quarter of an hour by a USGS gauge located near Richmond, Virginia. The implementation of a fresh water point source for the James River was necessary in order to correctly estimate the water level in the wetlands located around the riverbanks.

3.3 SWAN Model Set up

In SWAN the waves and the non-linear phenomena generated during their propagation in the surf zone are described with the two-dimensional wave action density spectrum. The reason

why the action density spectrum $N(\sigma,\theta)$ rather than the energy density spectrum $E(\sigma,\theta)$ is considered relates to the presence of currents, in which action density is conserved whereas energy density is not. The evolution of the wave spectrum in the geographical space x with time t is described by the spectral action balance equation which for Cartesian coordinates is (e.g., Hasselmann et al., 1973):

$$\frac{\partial}{\partial t}N + \frac{\partial}{\partial x}c_x N + \frac{\partial}{\partial y}c_y N + \frac{\partial}{\partial \sigma}c_\theta N + \frac{\partial}{\partial \theta}c_\theta N = \frac{S}{\sigma} \quad (5)$$

Equation (5) relates the change in wave action in time to the source term energy density ($S = S(\sigma,\theta)$) created by the effects of wave generation, dissipation (whitecapping, surf breaking and bottom friction) and non–linear wave-wave interaction. The term of the spectral action balance $\frac{\partial}{\partial t}N$ represents the local rate of change of action density in time, while $\frac{\partial}{\partial x}c_x N + \frac{\partial}{\partial y}c_y N$ estimates the propagation of action in geographical space in the x- and y- directions. The value $\frac{\partial}{\partial \sigma}c_\theta N$ quantifies the shifting of the relative frequency due to variations in depths and currents with propagation velocity in the σ- space. The $\frac{\partial}{\partial \theta}c_\theta N$ term represents depth-induced and current-induced refraction with propagation velocity θ- space). The expressions for these propagation speeds are taken from linear wave theory (Whitham et al., 1974; Mei et al., 1983; Dingemans et al., 1997).

3.3.1 Delft3D-FLOW – SWAN Coupling

Delft3D-FLOW and SWAN software were coupled to estimate the wave component in shallow water during the storm surge. Coupling is a computer process that involves the run of two different computational engines on the same grid. The grid identity allows both the computational engines to communicate exchanging information during the simulation time. The

coupling process is regulated by an external script, which contains the commands to run and stop the two computational engines.

In this case, the coupling process was implemented only for Model 1 and started with the execution of Delft3D-FLOW, which as previously explained estimates flow variables under space and time varying conditions. The computed variables were then stored in a communication file. According to an external script, every 0.12 seconds the computer stopped Delft3D-FLOW to activate the SWAN engine, which estimated the wave component based on the flow variables previously located in the communication file. Once the estimation of the wave component had been completed, the results were transferred once again in the communication file and used as input conditions for the reactivation of the Delft3D-FLOW. It is important to notice how the wave component computed by SWAN is related only to the time step at which Delft3D-FLOW was stopped and not to the entire 0.12 seconds running interval.

3.3.2 Boundary Conditions

The coupling process made the inputs for SWAN equal to the ones for Delft3D-FLOW. The two computational engines share the same grid, topography, bathymetry, wind and pressure data. The only exclusive input for SWAN consists in the wave boundary condition, which includes offshore wave data provided by the buoy station 44099 – Cape Henry historic during Hurricane Irene.

CHAPTER 4

RESULTS

4.1 Tide and storm surge validation without wave component

Prior to applying the model for future storm surge flooding, the model performance was validated with the observed storm surge from Hurricane Irene (2011). The model parameters were kept constant over the three levels of nesting. Sea water density was 1025 kg/m3, background atmospheric pressure was 1030 mbar, the bottom roughness was represented by the Manning coefficient which was assumed to be 0.03 for the first level of the model, and 0.02 for both the second and third levels. These values were obtained through tidal calibration. Horizontal eddy viscosity was kept the same as the default value of 1 m^2/s. All the boundary conditions in the model, such as bathymetry and initial water level have been specified at the corners of the grid cells, and the threshold depth for wetting and drying was 0.1 m. The vertical datum was NAVD88. Data from two NOAA tide gauges located at the Chesapeake Bay Bridge Tunnel (CBBT) and Sewells Point were used to validate the performance of the Delft3D model. The CBBT data was used to validate Model 1. The domain extent and grid resolution of Model 1 were selected such that the storm track through the Hampton Roads area was captured adequately while the grid had a high enough resolution to capture the storm and tide propagation into the Chesapeake Bay. As seen in Fig. 7(a), Model 1 results for Hurricane Irene and the tidal elevations prior to the storm compared well with the buoy data. The root mean square error (RMSE) was 0.156 m. The only notable discrepancy occured at two tidal cycles prior to the storm peak. According to NOAA, Hurricane Irene's radius was hard to estimate due to the larger than normal size dimension of the cyclone and the absence of a particularly intense inner core during August 26-27 (Lixion et al., 2011). Nevertheless, the model was able to capture water

levels at the storm peak very well. Model 2 was validated using the Sewells Point tide gauge. As seen in Fig. 7(b), the model results for tidal elevation and the storm surge compared well with the data. The RMSE was 0.155 m. The slight discrepancy observed at the peak may be attributed to the inadequacy in representation of the shallow bathymetry in the model. At the time of this thesis, no tide gauges data were available in the domains of Model 3; hence, the tide and storm surge validation of Model 3 were not possible. Therefore, the model was validated up to the first two levels of nesting.

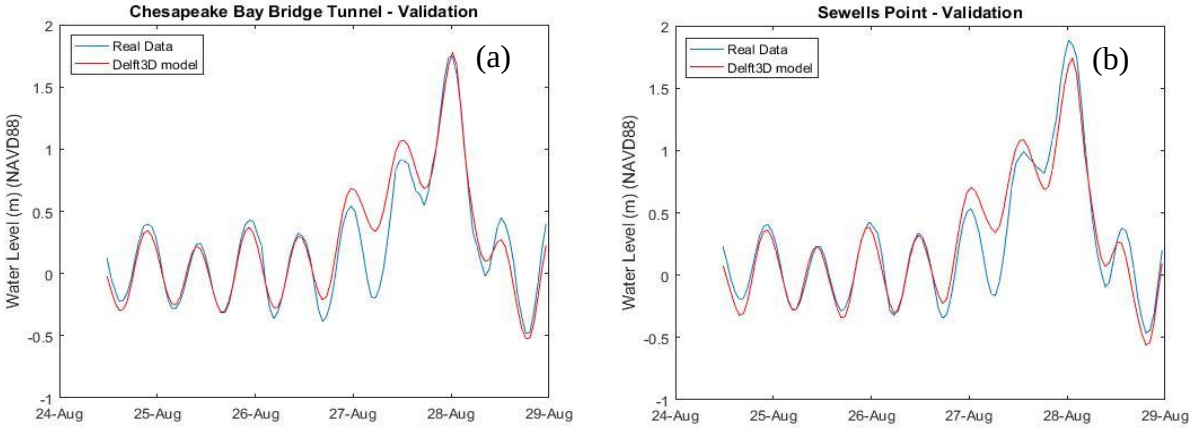

Fig. 7. Comparison between hydrodynamic model results for water level and the data from the tide gauge at (a) the Chesapeake Bay Bridge and (b) Sewells Point Tunnel during Hurricane Irene (2011).

4.2 Tide and storm surge validation with wave component

The SWAN engine was set to account for the different types of physical processes such as wind stress on water surface, wave breaking ($\alpha = 1$ and $\gamma = 0.78$), non-liner triad interactions ($\alpha = 0.1$ and $\beta = 2.2$), and the energy lost due to bottom friction, estimated using JONSWAP with a roughness coefficient of 0.067. Quadruteles and whitecapping processes were also included in the simulation. Waves propagated in the spectral space according to refraction and frequency

shift and were computed with an accuracy criterion of relative change Hs-Tm01 of 0.02 and percentage of grid points of 98%.

Fig. 8 shows the comparison between Delft3D-FLOW with and without SWAN coupling compared to real measurements from the NOAA tide gauges located at CBBT. Since the difference between the two models is minimal, the results were obtained without coupling due to the longer computation time that this process requires.

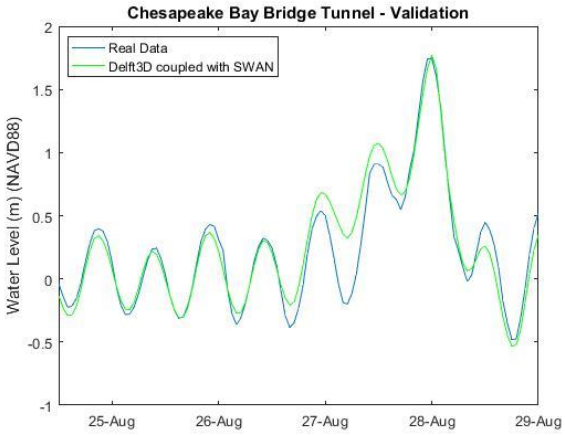

Fig. 8. Comparison between hydrodynamic model with and without waves and the data from the tide gauge at the Chesapeake Bay Bridge Tunnel during Hurricane Irene (2011).

4.3 Storm surge under future sea level rise condition

The primary goal for this thesis was to develop a hydrodynamic model that could assess bridge vulnerability to storm surge inundation under SLR. All eight flood-prone bridges were selected because they were vulnerable to direct storm surge inundation. The difference between direct and indirect vulnerability was related to the drainage capacity provided in the considered location. The combination of high water due to storm surge and high tide submerge the outlets and cause the stormwater to back up in the drainage system and prevent the stormwater infrastructure from functioning properly. This effect creates or contributes to flooding even in

areas not directly inundated by storm surge. Three SLR projections presented in a recent NOAA report (Sweet et al, 2017) were considered. This report added an extreme flooding scenario to earlier projections. The selected projections were based on the intermediate-low (IL), intermediate-high (IH), and extreme SLR scenarios. Table 3 summarizes these estimates for 2050 and 2100, the two time frames considered in this study. It should be noted that the study can readily be extended to other SLR estimates. The effect of SLR was added to the model by increasing the water level to the desired values at the boundaries of Model 1 and allowed enough time for the sea level change to propagate throughout the domain. This would change the boundary conditions for Models 2 and 3. In addition to flooding depth, the hydrodynamic model allowed for estimation of the flood duration at observation points placed during the model set up.

Table 3. SLR scenarios used in storm surge simulations. The values are based on NOAA Technical Report NOS CO-OPS 083 (Sweet, 2017).

Sea Level Rise (m)	**2050**	**2100**
Intermediate-Low	0.24	0.5
Intermediate-High	0.44	1.5
Extreme	0.63	2.5

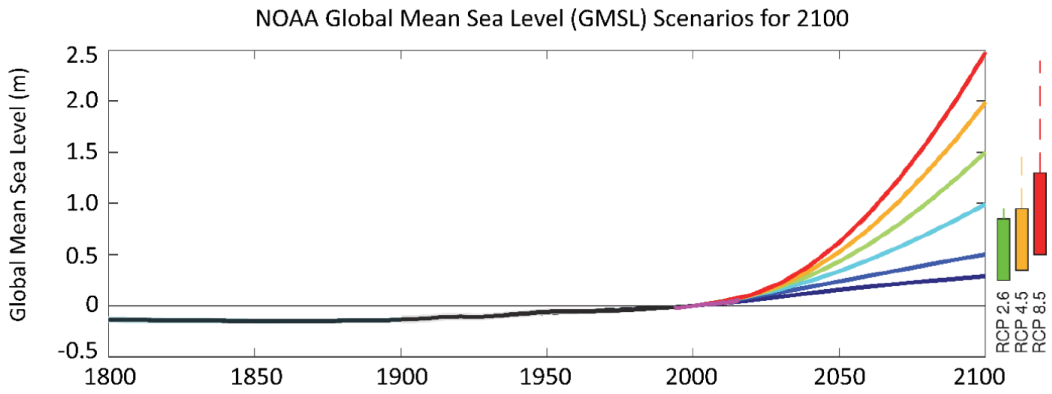

Fig. 9. Sea Level rise scenario from NOAA Technical Report NOS COOPS083 (Sweet, 2017).

The first flood-prone bridge studied was on US 58 Brambleton Ave. In Fig. 10, the extent of storm surge flooding driven by Hurricane Irene (2011) in the Hague area is depicted under correct sea level conditions and for selected SLR scenarios for 2050 and 2100. Highlighted as green, flooded under current sea level, the west side of the bridge was particularly vulnerable.

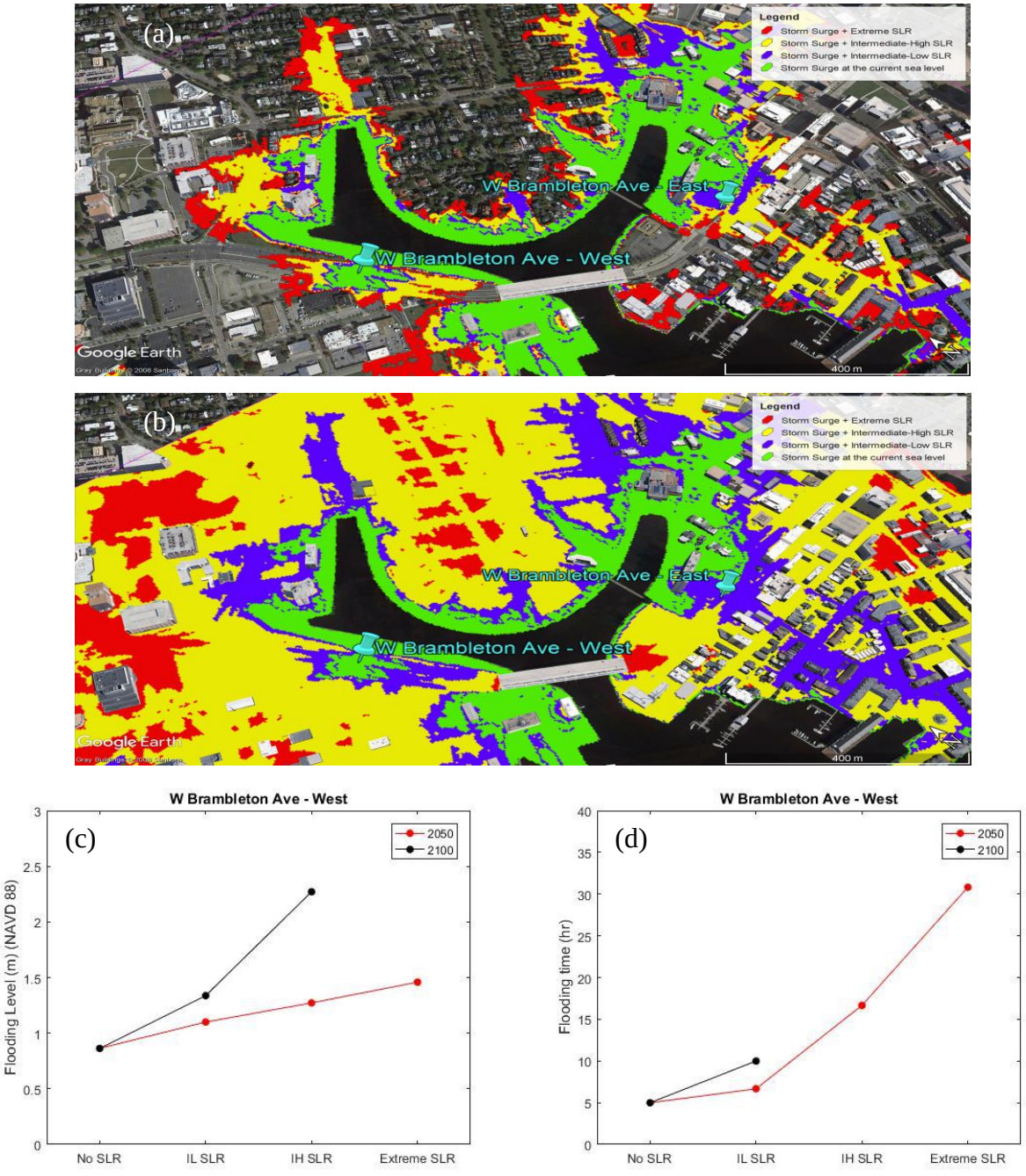

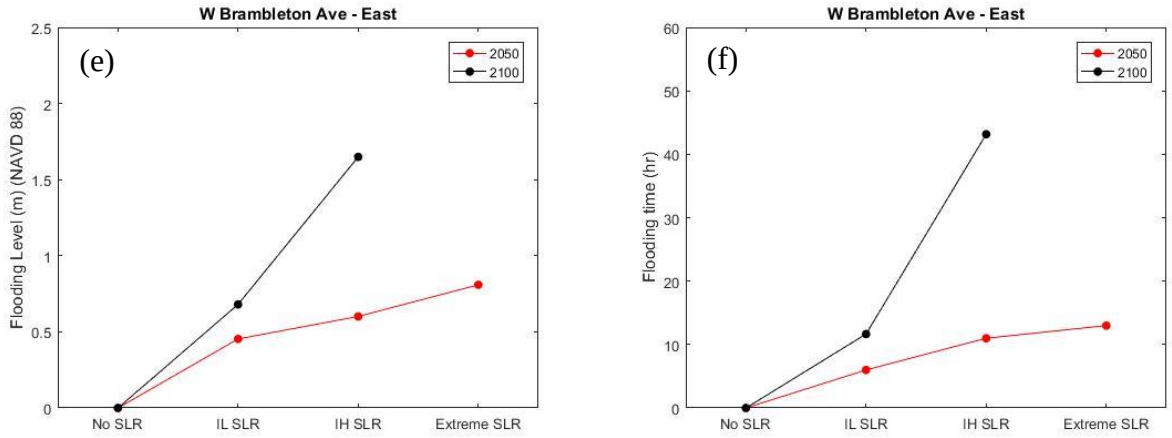

Fig. 10. Result of the Delft3D hydrodynamic model for storm surge flooding at US 58 Brambleton Ave for (a) 2050 and (b) 2100. The blue markers show the location where the model provides high resolution output of (c, e) flooding level and (d, f) duration.

All the values present in the plots of Fig. 10 provide the measurements for flood duration and intensity; Tables 4 and 5 respectively report the data for all locations. In estimating the flood duration, the location was assumed to be flooded once the total water level (storm surge + tide + SLR) was higher than the elevation of the point. It should be noted that the hydrodynamic model did not account for drainage, infiltration, or evaporation; hence, if the water created a pond at a low-lying spot after the storm surge receded, the water level would remain at a constant non-zero value at that location. Therefore, the flooding was considered to be completed once the water level subsided and reached a value constant with time, even if the value was not zero. Observation points for flooding intensity and duration were inputted during the model set up at roads that provide access to the bridges. Flooding maps obtained through Model 2 and 3 differ in terms of accuracy due to the refinement level of the hydrodynamic grid. While a grid resolution of 2.5-3.5 × 2.5-3.5 m^2 can better capture topography and, thus, flooding for small neighborhood roads, a resolution of 9-10 × 9-10 m^2 revealed to be sufficient to reproduce the large access road elevations.

James River was the second critical spot studied. Due to its length, the bridge could not be included in only one Model 3 domain, it had to be separated into two hydrodynamic models. Fig. 11 shows the extent of the flooding on both sides; the results indicate that the entry road located in Isle of Wight was the more vulnerable side of the bridge.

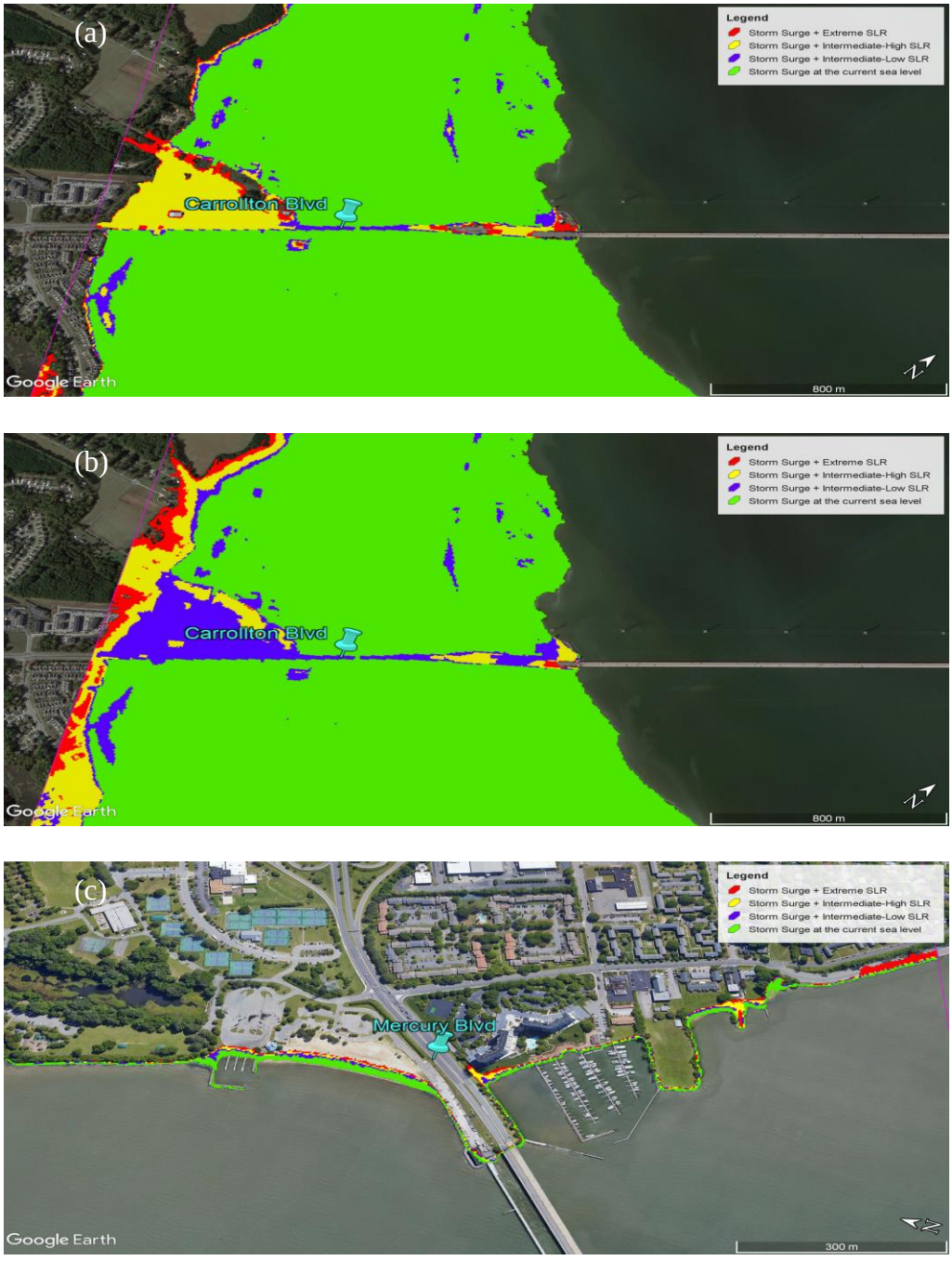

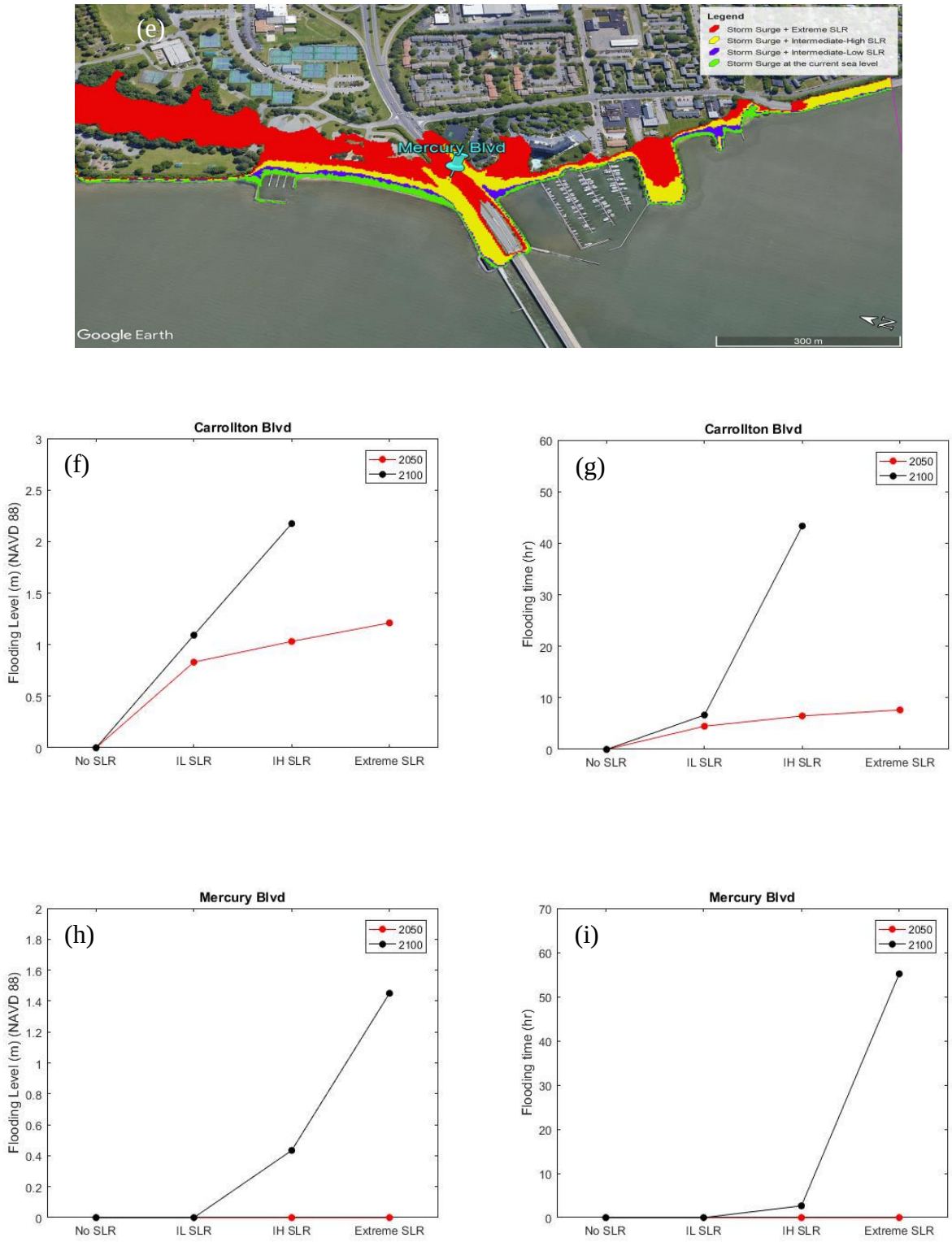

Fig. 11. Result of the Delft3D hydrodynamic model for storm surge flooding at the two banks of James River for (a) 2050 and (b) 2100. The blue marker shows the location where the model provides high resolution output of (f, h) flooding level and (g, i) duration

I-264 and US Military Highway bridges were included in the same refined area of Model 2. Fig. 12 shows the extent of the flooding at both bridges and according to the following tables, the south side of the US 13 Military Highway bridge was the most vulnerable side of the bridge; since it flooded starting at the intermediate-high (IH) SLR projection of 2050.

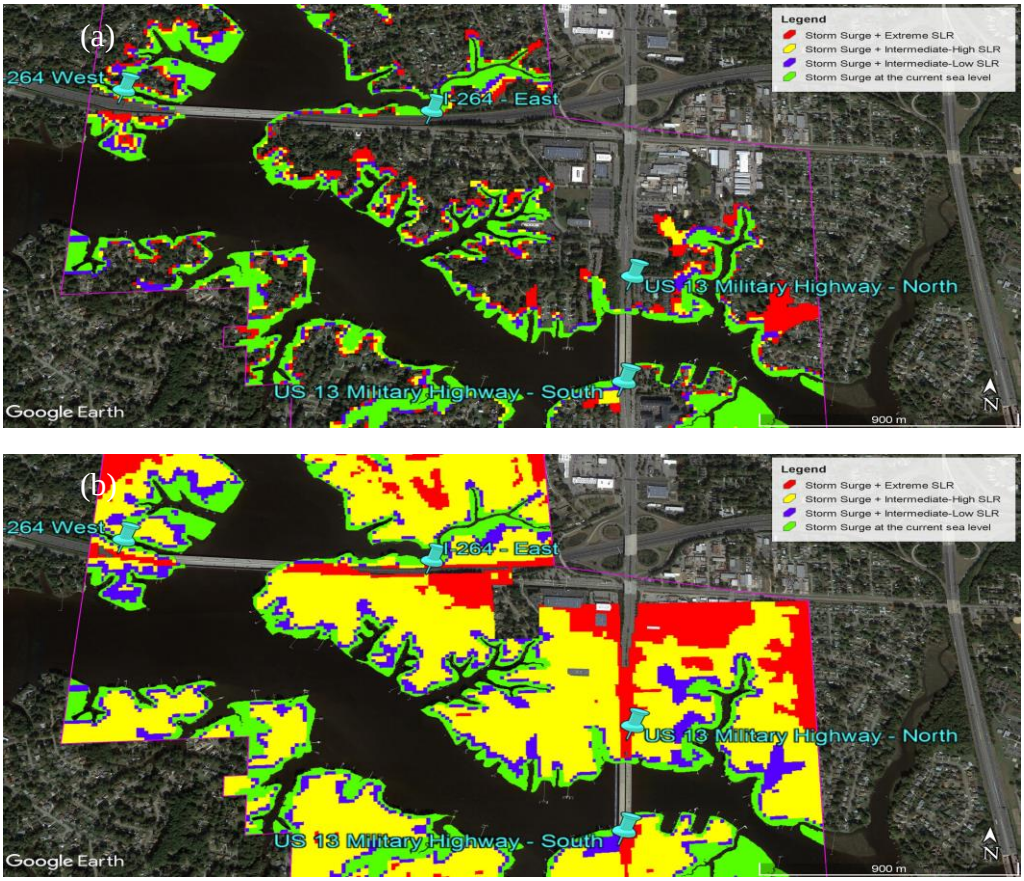

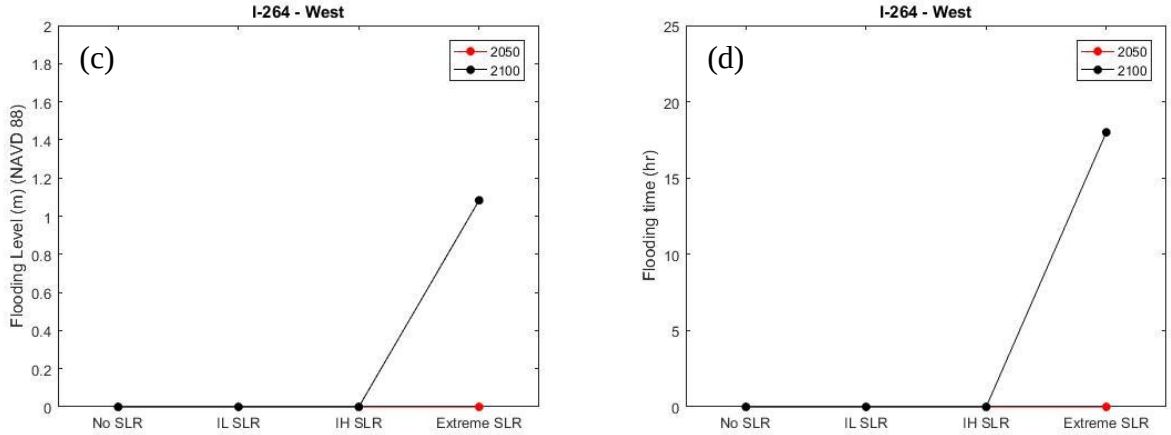

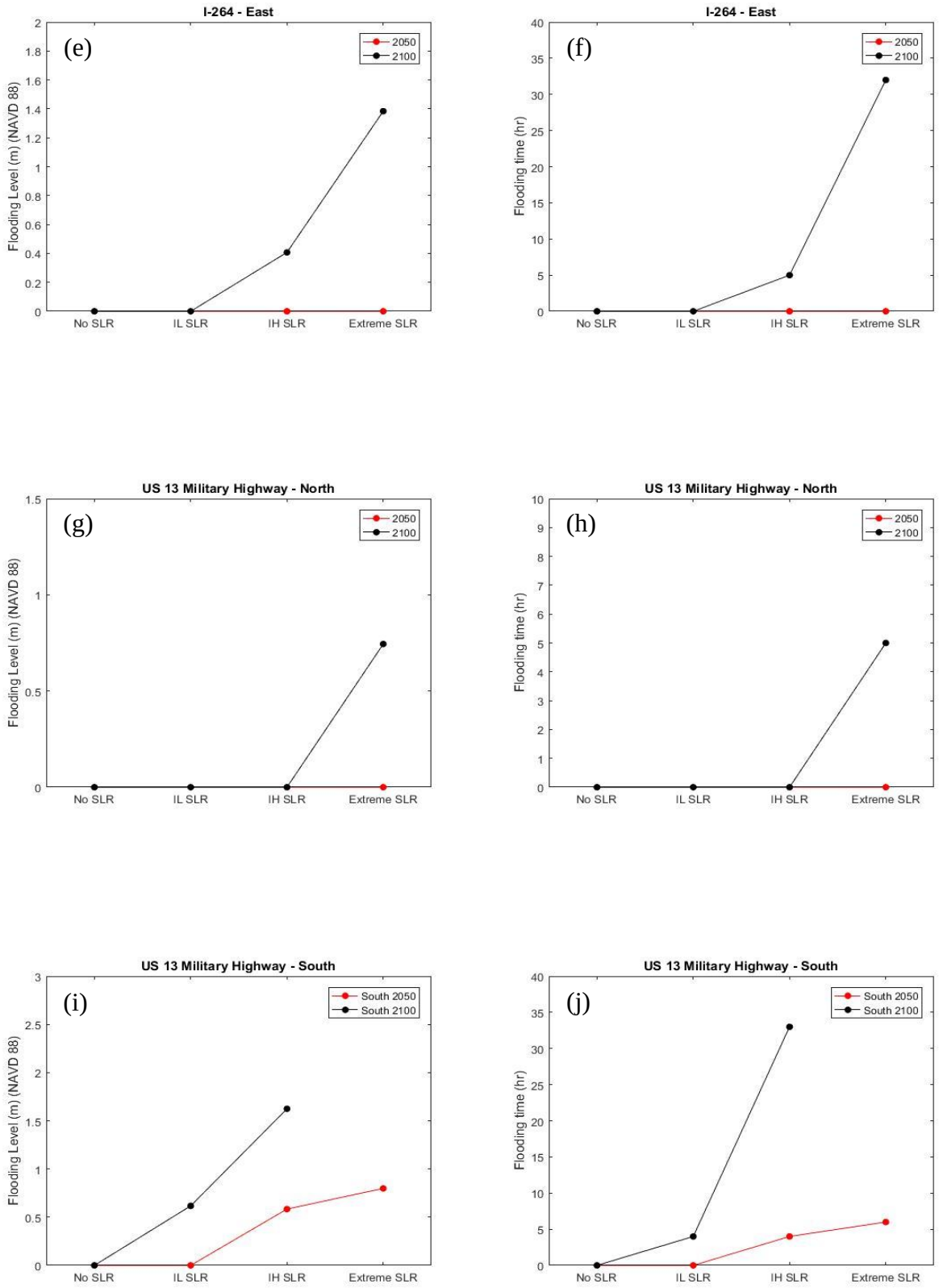

Fig. 12. Result of the Delft3D hydrodynamic model for storm surge flooding at I-264 and US Military Highway bridges for (a) 2050 and (b) 2100. The blue marker shows the location where the model provides high resolution output of (c, e, g, i) flooding level and (d, f, h, j) duration

Shore Dr. was the more exposed bridge included in this study. Compared to the rest of the bridges, which are located in more sheltered areas around rivers banks, Shore Dr. connects two sides of an inlet which grants access for navigation in the Chesapeake Bay. Fig. 13 illustrates the vulnerability of this location, particularly on the west side.

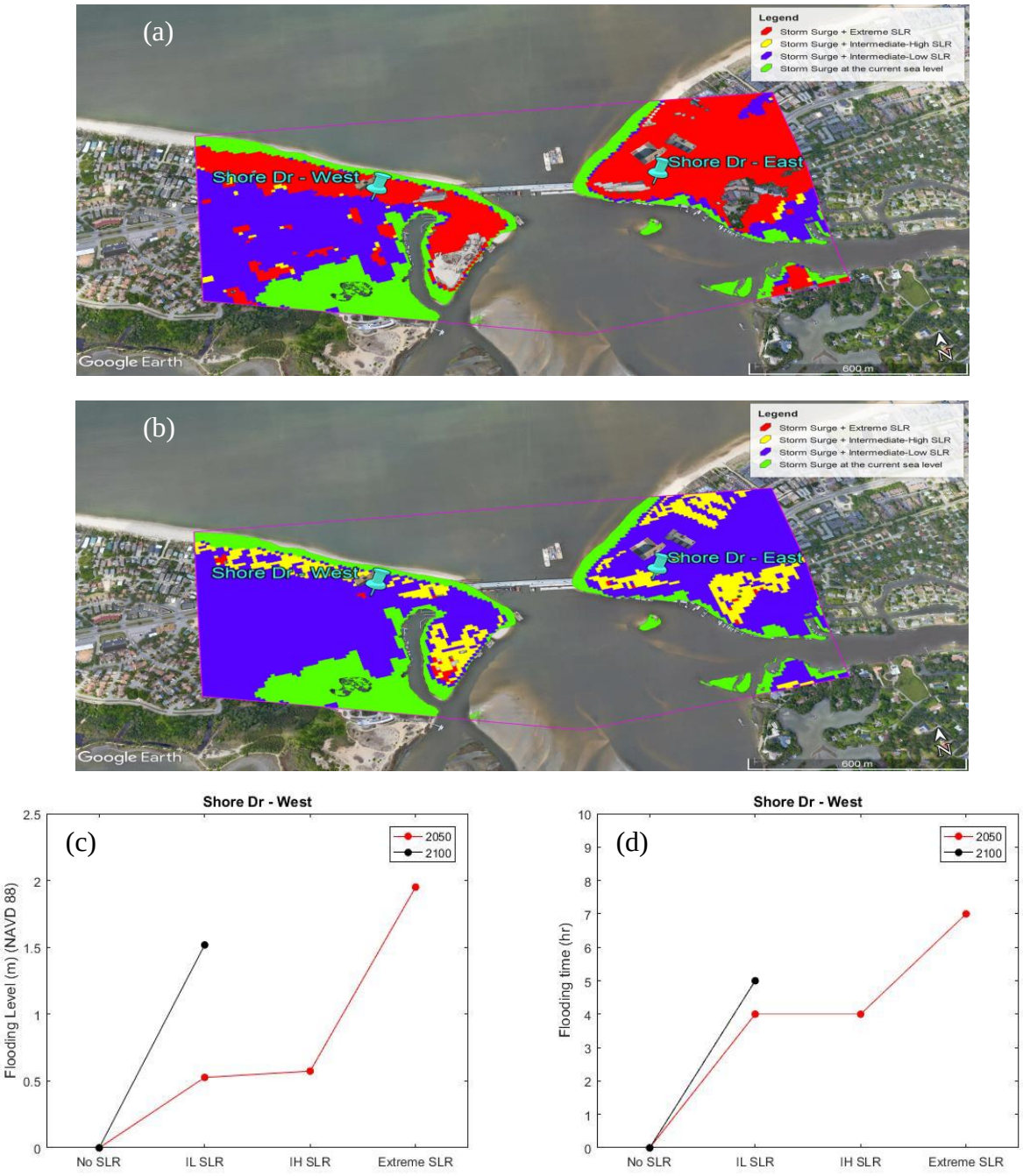

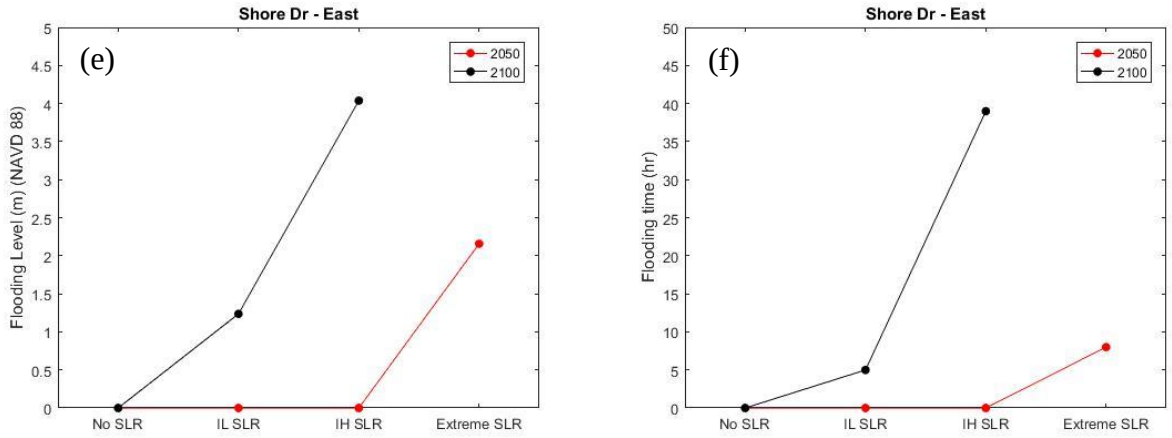

Fig. 13. Result of the Delft3D hydrodynamic model for storm surge flooding at Shore Dr. bridge for (a) 2050 and (b) 2100. The blue marker shows the location where the model provides high resolution output of (c, e) flooding level and (d, f) duration.

VA 337 – Hampton Blvd bridge is an important point of connection between Norfolk downtown and the naval base. The results plotted in Fig. 14 show the extent of flooding and identify the south side as the most vulnerable to storm surge since the observation point registers flooding starting at the current sea level.

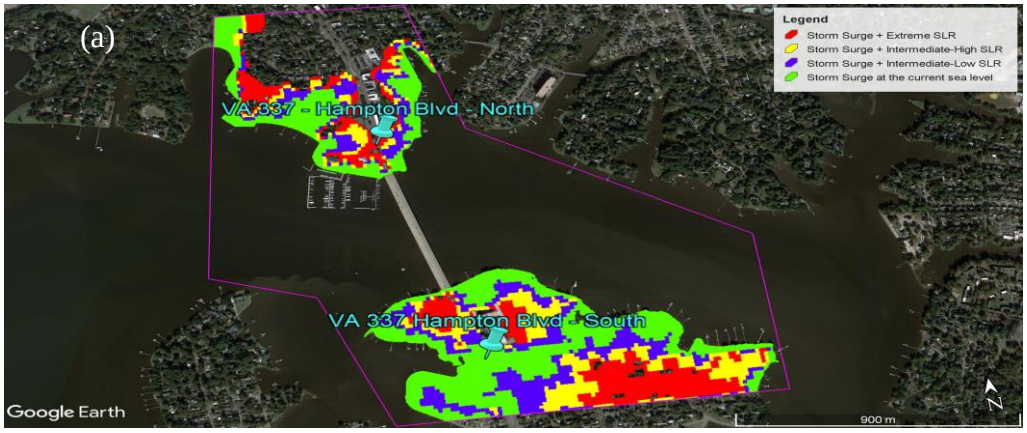

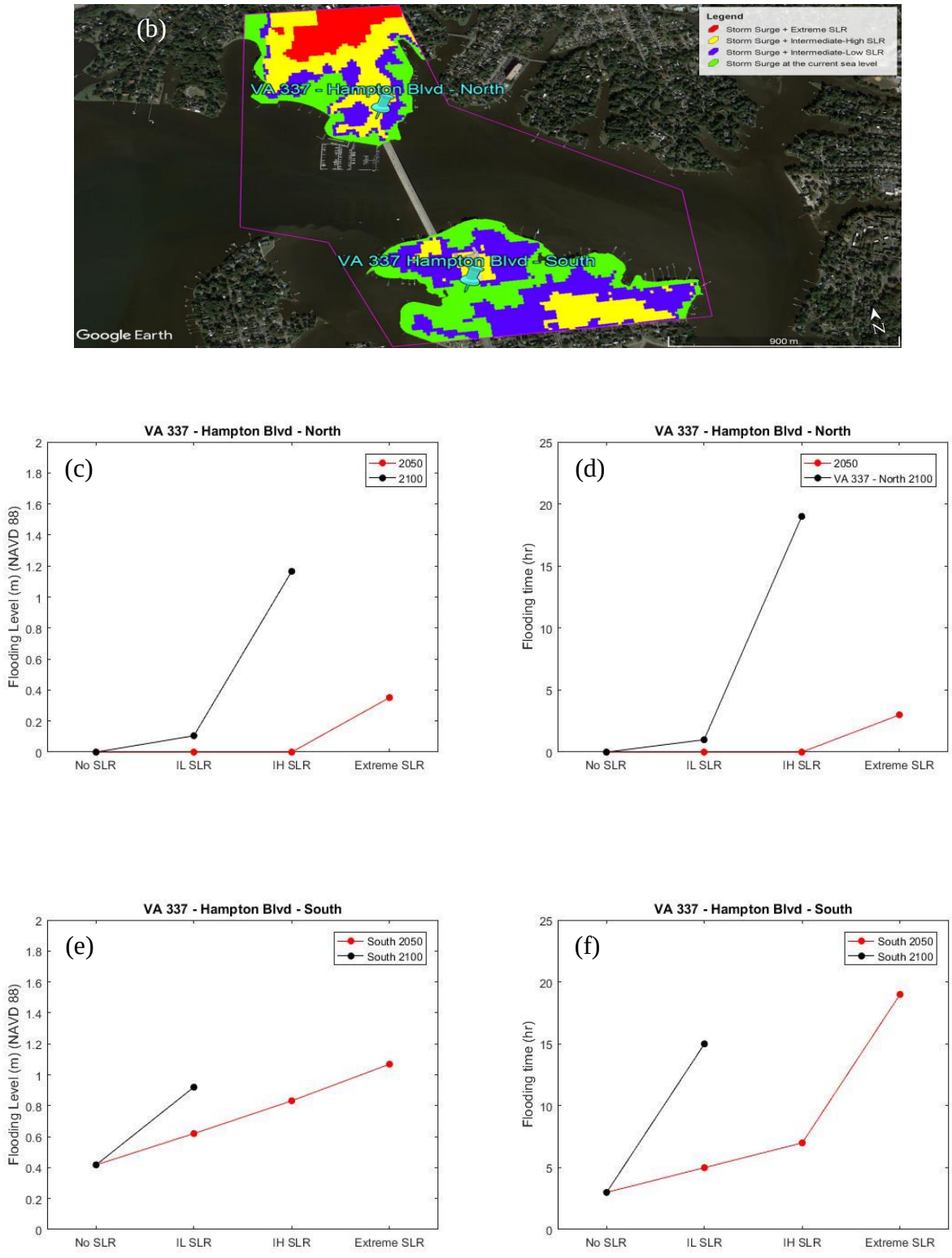

Fig. 14. Result of the Delft3D hydrodynamic model for storm surge flooding at VA 337 – Hampton Blvd bridge for (a) 2050 and (b) 2100. The blue marker shows the location where the model provides high resolution output of (c, e) flooding level and (d, f) duration.

US 460 is a small bridge which grants the access to one of the historic neighborhoods of Norfolk, the Colonial Place. The results visible in Fig. 15 indicate the north side to be more vulnerable to flooding under SLR projections for 2050. The bridge resulted as highly vulnerable to SLR predictions for 2100 since both sides got flooded.

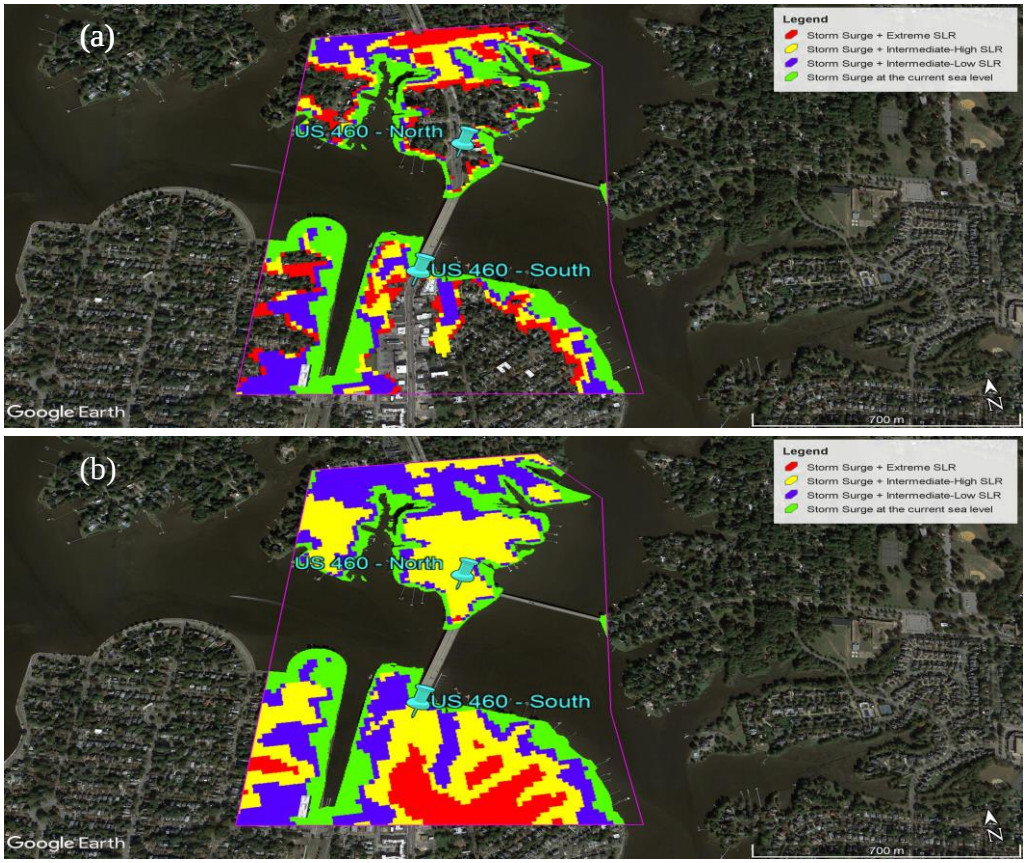

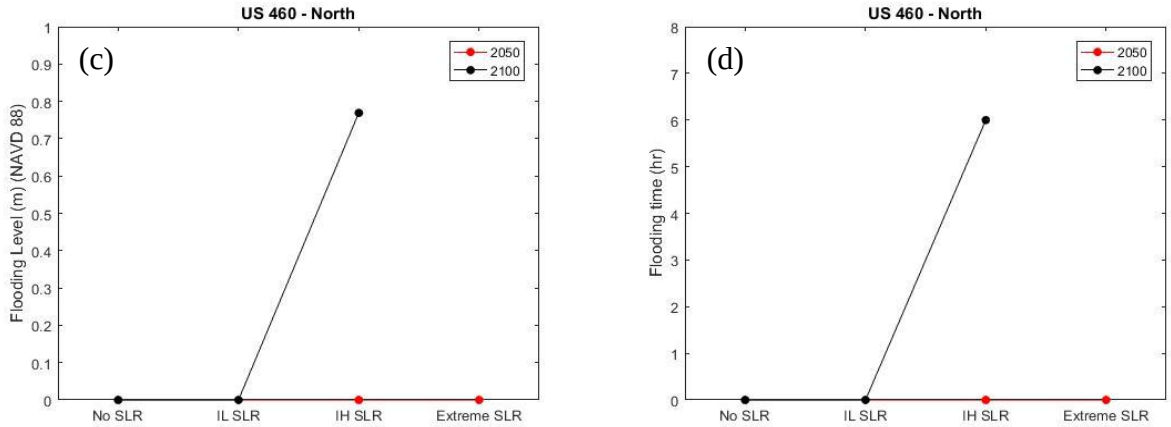

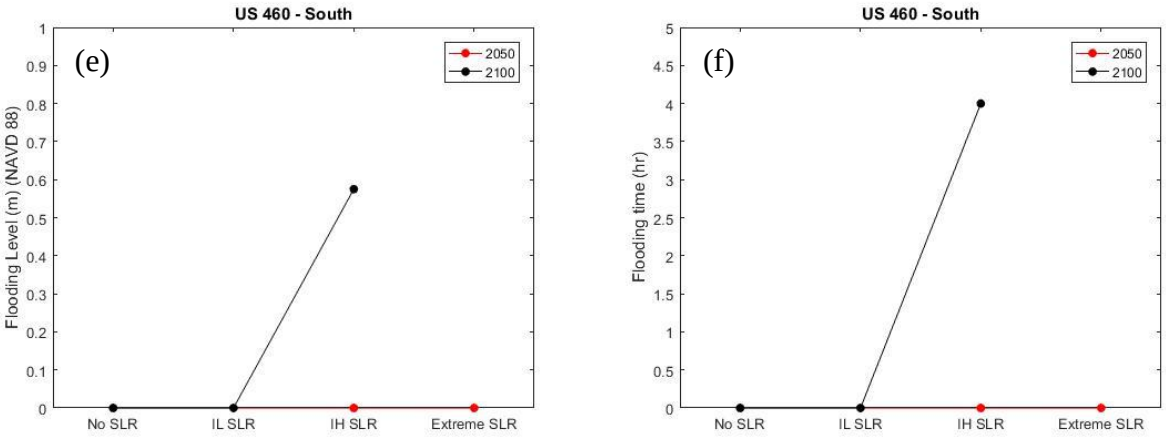

Fig. 15. Result of the Delft3D hydrodynamic model for storm surge flooding at US 460 bridge for (a) 2050 and (b) 2100. The blue marker shows the location where the model provides high resolution output of (c, e) flooding level and (d, f) duration.

I-64 WB/EB is one of the many bridges across the Elizabeth River that connects two sides of the City of Chesapeake. The Virginia Department of Transportation classified this bridge as obsolete for its geometric standard, and there are plans for it to be replaced in the near future. According to Fig. 16, the bridge suffered major flooding starting at the intermediate-high projection of 2100.

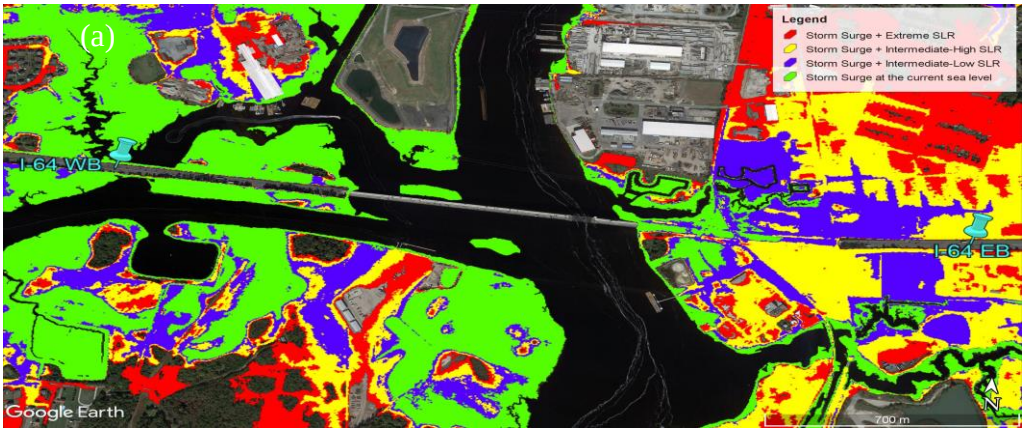

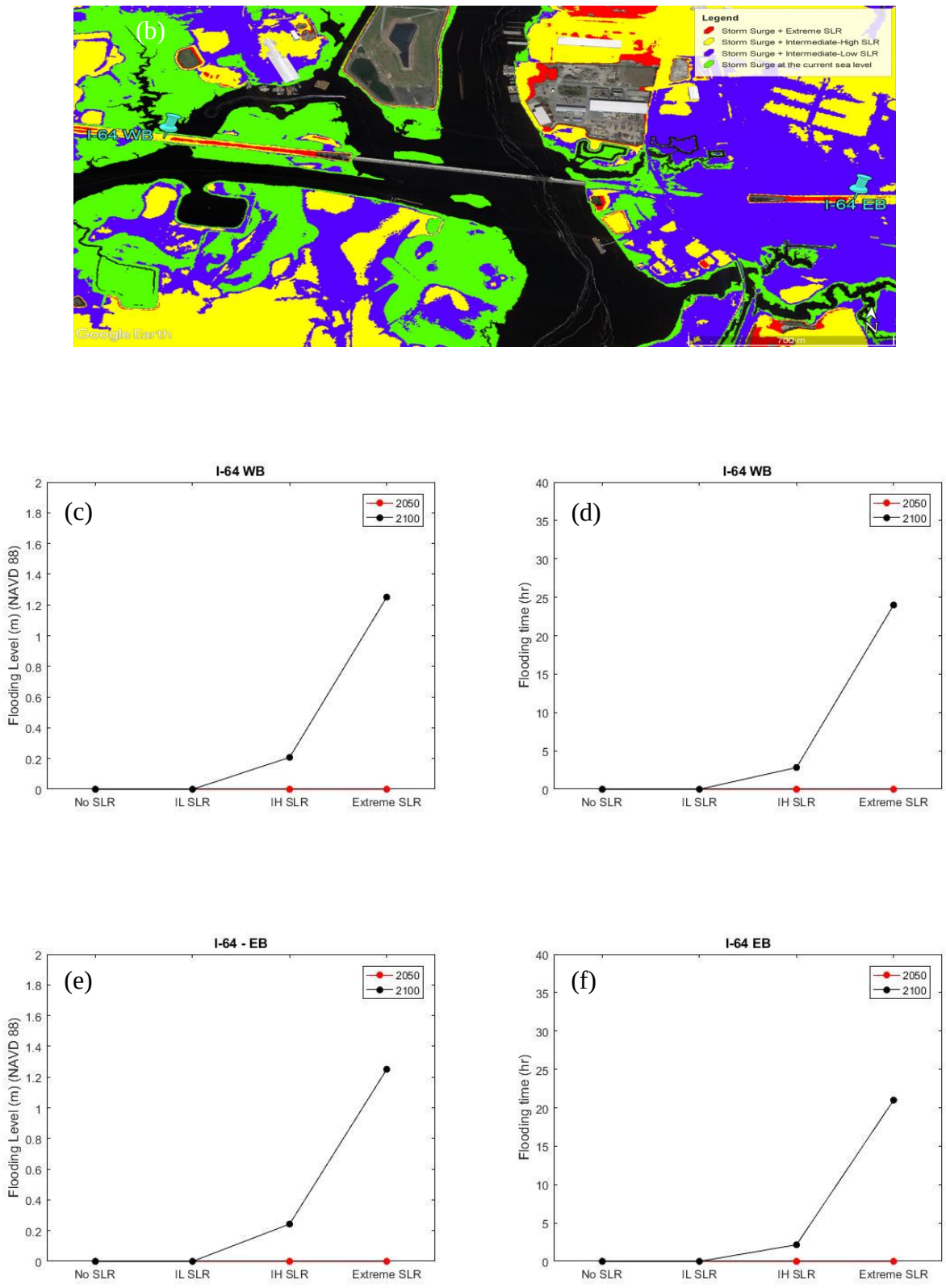

Fig. 16. Result of the Delft3D hydrodynamic model for storm surge flooding at I-64 WB/EB bridge for (a) 2050 and (b) 2100. The blue marker shows the location where the model provides high resolution output of (c, e) flooding level and (d, f) duration.

4.4 Hydrodynamic model compared to the "bathtub" approach

To highlight the difference between the developed hydrodynamic model and the bathtub approach, the results under the same water level conditions (2.1 m) were compared. Fig. 17 shows how the bathtub model significantly overestimated the extent of the flooding in streets farther from the waterfront, which would be clear based on the hydrodynamic model. Estimates from the "bathtub" approach have been done using the Delft3D model developed for this thesis. It is important to note how using the same model for both approaches gave the results a common base for comparison. Furthermore, Delft3D-FLOW engine accounted for hydraulic connectivity; therefore, only areas with lower elevation than the projected sea level and hydraulically connected to the waterfront got flooded.

Fig. 17. Comparison between the storm surge model estimates for inundation extent under intermediate-high SLR in 2050 (yellow) and estimates based on the bathtub approach (red).

Table 4. Flooding level (m) estimated by the model at selected locations.

Flooding Level (m) at locations	*Current Sea Level*	*2050 Scenarios*			*2100 Scenarios*		
		Intermediate-Low	*Intermediate-High*	*Extreme*	*Intermediate-High*	*Intermediate-Low*	*Extreme*
Carrollton Blvd	*0*	*0.83*	*1.03*	*1.21*	*1.09*	*2.17*	*Continues Flooding*
Mercury Blvd	*0*	*0*	*0*	*0*	*0*	*0.43*	*1.45*
I-264 West	*0*	*0*	*0*	*0*	*0*	*0*	*1.08*
I-264 East	*0*	*0*	*0*	*0*	*0*	*0.41*	*1.38*
US 13 Military Highway - North	*0*	*0*	*0*	*0*	*0*	*0*	*0.74*
US 13 Military Highway - South	*0*	*0*	*0.58*	*0.79*	*0.62*	*1.62*	*Continues Flooding*
US 460 - North	*0*	*0*	*0*	*0*	*0*	*0.77*	*Continues Flooding*
US 460 - South	*0*	*0*	*0*	*0*	*0*	*0.57*	*Continues Flooding*
VA 337 – Hampton Blvd North	*0*	*0*	*0*	*0.35*	*0.11*	*1.17*	*Continues Flooding*
VA 337 – Hampton Blvd - South	*0.42*	*0.62*	*0.83*	*1.07*	*0.92*	*Continues Flooding*	*Continues Flooding*
Shore Dr. - West	*0*	*0.53*	*0.57*	*1.95*	*1.52*	*Continues Flooding*	*Continues Flooding*
Shore Dr. - East	*0*	*0*	*0*	*2.16*	*1.24*	*4.03*	*Continues Flooding*
W. Brambleton Ave - West	*0.86*	*1.10*	*1.27*	*1.46*	*1.34*	*16.67*	*Continues Flooding*
W. Brambleton Ave - East	*0*	*0.45*	*0.60*	*0.81*	*0.68*	*1.65*	*Continues Flooding*
I-64 WB	*0*	*0*	*0*	*0*	*0*	*0.21*	*1.25*
I-64 EB	*0*	*0*	*0*	*0*	*0*	*0.24*	*1.26*

Table 5. Flooding time (hr) estimated by the model at selected locations.

Flooding time (hr) at locations	*Current Sea Level*	*2050 Scenarios*			*2100 Scenarios*		
		Intermediate-Low	*Intermediate-High*	*Extreme*	*Intermediate-High*	*Intermediate-Low*	*Extreme*
Carrollton Blvd	*0*	*4.5*	*6.5*	*7.67*	*6.67*	*43.34*	*Continues Flooding*
Mercury Blvd	*0*	*0*	*0*	*0*	*0*	*2.67*	*55.17*
I-264 West	*0*	*0*	*0*	*0*	*0*	*0*	*18*
I-264 East	*0*	*0*	*0*	*0*	*0*	*5*	*32*
US 13 Military Highway - North	*0*	*0*	*0*	*0*	*0*	*0*	*5*
US 13 Military Highway - South	*0*	*0*	*4*	*6*	*4*	*33*	*Continues Flooding*
US 460 - North	*0*	*0*	*0*	*0*	*0*	*6*	*Continues Flooding*
US 460 - South	*0*	*0*	*0*	*0*	*0*	*4*	*Continues Flooding*
VA 337 – Hampton Blvd North	*0*	*0*	*0*	*3*	*1*	*19*	*Continues Flooding*
VA 337 – Hampton Blvd - South	*3*	*5*	*7*	*19*	*15*	*Continues Flooding*	*Continues Flooding*
Shore Dr. - West	*0*	*4*	*4*	*7*	*5*	*Continues Flooding*	*Continues Flooding*
Shore Dr. - East	*0*	*0*	*0*	*8*	*5*	*39*	*Continues Flooding*
W. Brambleton Ave - West	*5*	*6.67*	*16.7*	*30.83*	*5*	*10*	*Continues Flooding*
W. Brambleton Ave - East	*0*	*6*	*11*	*13*	*11.67*	*43.16*	*Continues Flooding*
I-64 WB	*0*	*0*	*0*	*0*	*0*	*2.83*	*24*
I-64 EB	*0*	*0*	*0*	*0*	*0*	*2.17*	*21*

CHAPTER 5

CONCLUSIONS

The objective of this research was to improve our understanding of the vulnerability of the transportation infrastructure in the Hampton Roads region to storm surge flooding under SLR. The study was focused on critical coastal bridges that are under higher risk of inundation due to combined effects of storm surge and SLR. To conduct the vulnerability assessment, a high-fidelity hydrodynamic model was developed based on the Delft3D modeling suite. Eight flood-prone locations were identified to study the impact of storms; the model was developed at three levels of nesting with spatial resolutions varying from 200 m to 2.5 m. The combined computational times of nested Models 1 to 3 was between 48 and 72 hours, depending on the level 3 model. The required computational time to obtain flooding estimates for bridges that have a locally refined grid in the level 2 model was much smaller (around 12 hours). Based on comparison with tide gage data at CBBT, the maximum flooding level and duration in the model that included waves was comparable to the model without the wave component. On the other hand, the computation time for simulation with the wave module was considerably larger. Therefore, the wave module was not included in simulations that were used to estimate flooding level and duration. Three different SLR scenarios, namely intermediate-low, intermediate-high, and extreme SLR were selected and storm surge flood maps were developed for a historic hurricane for the present sea level as well as the projected SLR at 2050 and 2100. The hurricane was defined using the parameters of Hurricane Irene (2011). The plots included in Fig. 10-16 show that increase in flooding intensity and duration are nonlinear to the increase in water level, which was a result of the flow dynamics process considered by Delft3D. The bridges identified by the model as the most vulnerable to flooding were VA 337 – Hampton Blvd and W.

Brambleton Ave; according to Table 4, they got flooded under the current sea level condition. Shore Dr., James River, US 13 Military Highway and VA 337 – Hampton Blvd bridges flooded under SLR projection for 2050, which indicates their potential vulnerability in the near future. On the other hand, being flooded only during the high SLR projections for 2100, US 460 and I-64 WB/EB appear to be the only locations selected that would suffer limited climate change consequences for almost another century. According to Tables 4 and 5, it should be noted how the extreme scenario projection for 2100 would have devastating consequences on the transportation infrastructures of the Hampton Roads region since it would completely submerge both accesses for five of the eight bridges selected.

Under the same water level condition, the results of the hydrodynamic model for the Hague neighborhood were compared to the widely used "bathtub" approach in a GIS model. The results indicate that the "bathtub" approach significantly overestimated the extent of the flooding in the selected area. This highlights the importance of the hydrodynamic analysis to estimate the storm surge. The Delft3D modeling suite has several modules that can be used to extend the present study beyond hydrodynamic analysis of storm surge. The present study does not take into account the effect of waves, and storm water runoff, which can potentially affect the results.

The results of this study on the extent, intensity, and duration of flooding under different SLR projections would enable more accurate design and implementation of flood mitigation measures, such as seawalls or storm water infrastructure, and can inform planning and management of traffic flow in the transportation network in the region.

CHAPTER 6

RECOMMENDATION

The present study can be improved in several ways. Comparison between model results and data shows that the model can satisfactorily predict water level in the Chesapeake Bay during tidal cycles and extreme weather conditions caused by Irene-like storms. At the time of this thesis, no tide gauges were available within the Model 3 domains; therefore, no proper validation was possible for the I-64 WB/EB, US 17, VA 337, US 58 Brambleton Ave and James River Bridge locations. The main source of error for Model 3 may be introduced by the vicinity of the domain boundaries, which can cause a negative interaction between the boundary conditions. The City of Norfolk has recently installed a tide gauge in the Hague area that could be used to validate level 3 models in the future.

The accuracy of model predictions for flooding over land is also not clear as there was no such data available for comparison at the time of this study. It would be recommended to measure water level over land during storm events and compare the model with such data. In addition, the Delft3D model estimates flow variables solving shallow water equations, which neglects the vertical acceleration component. In a flooded environment, the vertical acceleration component generated by the water flowing around submerged urban structures may become significant and no longer negligible. Furthermore, the effects of waves are not included in the model. Although the results from Model 1 at CBBT suggests that the impact of waves on storm surge may not be significant, they may provide a small contribution to the flooding extension in land. The flooding maps have a sensitivity between wet and dry of 10 cm; therefore, only areas with an equal or larger value compared to this threshold are considered as flooded by Delft3D.

In addition to increased flooding risk, SLR can result in changes in morphology through erosion and a general shoreward shifting of swallow water coastal processes, such as breaking waves and currents. SLR effects on the shoreline can be simulated using the sediment transport and morphological module in the Delft3D modeling suite. These impacts of SLR were beyond the scope of this thesis but can be the subject of a future study.

Although the present study focuses mainly on bridges, the developed model can be applied to other sensible spots located in coastal areas vulnerable to storm surge and SLR or, on a larger scale, even include the entire transportation network in Hampton Roads, albeit in lower spatial resolution. This approach can enable us to identify the locations in Hampton Roads that are vulnerable to storm surge and SLR.

REFERENCES

Ashton, A.D., J.P. Donnelly, and R.L. Evans, "A discussion of the potential impacts of climate change on the shoreline of the northeastern USA". *Mitigation and Adaptation Strategies got Global Change*, vol. 13(7), pp 719-743, 2008.

Atkinson, J., J. McKee Smith, and C. Bender, "Sea-Level Rise Effects on Storm Surge and Nearshore Waves on the Texas Coast: Influence of Landscape and Storm Characteristics." *Journal of Waterway, Port, Coastal, and Ocean Engineering*, vol. 139, No. 2, pp. 98-117, 2013.

Bender, M. A., T. R. Knutson, R. E. Tuleya, J. J. Sirutis, G. A. Vecchi, S. T. Garner, and I. M. Held, "Modeled Impact of Anthropogenic Warming on the Frequency of Intense Atlantic Hurricanes," *Science*, vol. 327, No. 5964, pp. 454–458, 2010.

Bhaskaran, P. K., Gayathri, R., Murty, P. L. N., Subba Reddy, B., and D. Sen, "A numerical study of coastal inundation and its validation for Thane cyclone in the Bay of Bengal," *Coastal Engineering*, 83,108–118, 2014.

Boon, J. D., J. M. Brubaker, and D. R. Forrest, "Chesapeake Bay land subsidence and sea level change", *App. Mar. Sci. and Ocean Eng*., Rep. No. 425, Va. Inst. of Marine Sci., Gloucester Point, VA., 2010.

Castrucci, L., and Tahvildari, N., "Hydrodynamic Modeling of Storm Surge Flooding in the Transportation Infrastructure in Southeast Virginia," *MTS/IEEE Oceans Conference*, Anchorage, AL, 2017

Casulli, V., and G. Stelling, "Semi-implicit sub-grid modeling of three-dimensional free-surface flows," *Intl. Journal for Numerical Methods in Fluid Dynamics*, vol. 67, pp 441-449, 2011.

Cialone, M. A., T. C. Massey, M. E. Anderson, A. S. Grzegorzewski, J. E. Jensen, A. Cialone, D. J. Mark, K. C. Pevey, B. L. Gunkel, T. O. McAlpin, "North Atlantic Coast Comprehensive Study (NACCS) Coastal Storm Model Simulations: Waves and Water Levels." *US Army Corps of Civil Engineering*, 252 p, 2015.

Climate Change Report, "Climate Change and the Chesapeake Bay: Challenges, Impacts, and the Multiple Benefits of Agricultural Conservation Work," 2007. http://www.cbf.org/document-library/cbf-reports/Climate-Change37bf.pdf

CSIRO, "Infrastructure and climate change risk assessment for Victoria, Commonwealth Scientific and Industrial Research Organization", 2007.

Dingemans, M. W., "Water Wave Propagation over Uneven Bottoms, Vol. 1 and 2." *Advanced Series on Ocean Engineering*, vol. 13, 1997.

Egbert, G. D., and S. Y. Erofeeva, "Efficient Inverse Modeling of Barotropic Ocean Tides." *J. Atmos. Oceanic Technol.*, vol. 19, pp. 183- 204, 2002.

Engelhart, S.E., W.R. Peltier, B.P. Horton, "Holocene relative sea-level changes and glacial isostatic adjustment of the U.S. Atlantic coast," *Geology Society of America,* vol. 39(8), 2011.

EPA, "Coastal Sensitivity to Sea-Level Rise A Focus on the Mid-Atlantic Region. U. S. C. C. S. P. a. t. S. o. G. C. Research". *U.S. Environmental Protection Agency, Climate Change Science Program:* 320, 2009.

Ezer, T., and L. P. Atkinson, "Accelerated flooding along the U.S. East Coast: On the impact of sea-level rise, tides, storms, the Gulf Stream, and the North Atlantic Oscillations", *Earth's Future*, vol. 2, pp 362–382, 2014. doi:10.1002/2014EF000252.

Governor's Commission on Climate Change, "Final Report: A Climate Change Action Plan" 2008.
http://www.sealevelrisevirginia.net/docs/homepage/CCC_Final_Report-Final_12152008.pdf

Gross, J. M., M. DeMaria, J. A. Knaff, and C. R. Sampson, "A new method for determining tropical cyclone wind forecast probabilities," *In Preprints, 26th Conf. on Hurricanes and Tropical Meteorology*, Miami, FL, Amer. Meteor. Soc. A (vol. 11), 2004.

Harvey, N., and R. Nicholls, "Global sea-level rise and coastal vulnerability". *Sustainability Science*, vol. 3(1), pp. 5-7, 2008.

Hasselmann, K., T. P. Barnett, E. Bouws, H. Carlson, D. E. Cartwright, K. Enke, J. Ewing, H. Gienapp, D. E. Hasselmann, P. Kruseman, A. Meerburg, P. M • uller, D. J. Olbers, K. Richter, W. Sell and H. Walden, "Measurements of wind wave growth and swell decay during the Joint North Sea Wave Project (JONSWAP)." *Deutsche Hydrographische Zeitschrift*, vol 8(12), pp. 48-131-133-138, 1973.

Holland, G. J., J. I. Belanger, and A. Fritz, "A revised model for radial profiles of hurricane winds," *Monthly Weather Review*, vol. 138(12), pp. 4393-4401, 2010.

Hu, K., Q. Chen, and H. Wang, "A numerical study of vegetation impact on reducing storm surge by wetlands in a semi-enclosed estuary", *Coastal Engineering*, vol. 95, pp. 66-76, 2015.
G. J. Holland, J. I. Belanger, and A. Fritz, "A revised model for radial profiles of hurricane winds," *Monthly Weather Review*, vol. 138(12), pp. 4393-4401, 2010.

Kleinosky, L. R., B. Yarnal and A. Fisher, "Vulnerability of Hampton Roads, Virginia to storm-surge flooding and sea-level rise," *Natural Hazards*, vol. 40(1), pp. 43-70, 2007.

Kont, A., J. Jaagus, R. Aunap, U. Ratas, and Reimo Rivis, "Implications of Sea-Level Rise for Estonia," *Journal of Coastal Research*, vol. 24(2), pp. 423-431, 2008.

Lin, N., K.A. Emanuel, J.A. Smith, and E. Vanmarcke, "Risk assessment of hurricane storm surge for New York City." *Journal of Geophysical Research*, 115: D18121. doi:10.1029/2009JD013630, 2010.

Li, H., L. Lin, and K. A. Burks-Cope, "Modeling of coastal inundation, storm surge, and relative sea-level rise at Naval Station Norfolk, Norfolk, Virginia, USA," *Journal of Coastal Research*, vol. 29(1), pp 18-30, 2012.

Lixion, A.A., and J. Cangialosi, "Tropical Cyclone Report Hurricane Irene (AL092011)", National Hurricane Center, 2011. http://www.nhc.noaa.gov/data/tcr/AL092011_Irene.pdf

Loftis, J. D., H. V. Wang, R. J. DeYoung and W. B. Ball, "Using Lidar Elevation Data to Develop a Topobathymetric Digital Elevation Model for Sub-Grid Inundation Modeling at Langley Research Center," *Journal of Coastal Research*, vol. 76, pp 134-148, 2016.

McInnes, K. L., I. Macadam, G. Hubbert, J. O'Grady, "An assessment of current and future vulnerability to coastal inundation due to sea-level extremes in Victoria, southeast Australia." *International Journal of Climatology*, vol. 33(1), pp 33-47, 2013

Murdukhayeva, A., P. August, M. Bradley, C. LaBash, and N. Shaw, "Assessment of Inundation Risk from Sea Level Rise and Storm Surge in Northeastern Coastal National Parks." *Journal of Coastal Research*, vol. 29(6a), pp. 1–16, 2013.

Neelz, S., and G. Pender, "Sub-gird scale parameterisation of 2D hydrodynamic models of inundation in the urban area." *Acta Geophysica*, vol. 55, pp 65–72, 2007.

Passeri, D. L., S. C. Hagen, S. C. Medeiros, M. V. Bilskie, K. Alizad, and D. Wang, "The dynamic effects of sea level rise on low-gradient coastal landscapes: A review", *Earth's Future*, vol. 3, pp. 159–181, 2015.

Mitchell, M., C. Hershner, J. Herman, D. Schatt, P. Mason, E. Eggington, L. Atkinson, E. Smith, B. McFarlene, J. White, B. Pennington, C. Smith, S. Stiles "Recurrent Flooding study for Tidewater Virginia", 2013.

Sallenger, A.H., Doran, K.S., and P.A. Howd, "Hotspot of accelerated sea-level rise on the Atlantic Coast of North America". *Nature Climate Change*, (published online 24 June, doi: 201210.1038/NCLIMATE1597), 2012.

Sadler, J. M., N. Haselden, K. Mellon, A. Hackel, V. Son, J. Mayfieldf, A. Blaseg and J. L. Goodall, "Impact of Sea Level Rise on Roadway Flooding in the Hampton Roads Region of Virginia." *Journal of Infrastructure Systems*, 2017.

Sebastian, A. G., J. M. Proft, C. J. Dietrich, W. Du, P. B. Bedient, and C. N. Dawson, "Characterizing storm surge behavior in Galveston Bay using the SWAN + ADCIRC model." *Coastal Engineering*, vol. 88, pp. 171–181, 2014.

Seenath, A., M. Wilson, K. Miller "Hydrodynamic versus GIS modelling for coastal flood vulnerability assessment: Which is better for guiding coastal management?" *Ocean & Coastal Management*, vol. 120, pp. 99-109

Sweet, W. V., R. E. Kopp, C. P. Weaver, J. Obeyskera, R. M. Horton, E. R. Thieler, and C. Zervas, "Global and regional sea level rise scenarios for the United States," NOAA Technical Report NOS CO-OPS 083, 2017.

Sto. Domingo, N.D., B. Paludan, H. Madsen, F. Hansen, and O. Mark, "Climate Change and Storm Surges: Assessing Impacts on Your Coastal City Through Mike Flood Modeling." *Copenhagen, Denmark: DHI Water, Environment and Health Report*, 11p, 2010.

Westerink, J.J., Luettich, R.A., Feyen, J.C., Atkinson, J.H., Dawson, C., Roberts, H.J., et al., "A basin to channel scale unstructured grid hurricane storm surge model applied to southern Louisiana." *Monthly Weather Review* 136 (3), 833–864, 2008.

Whitham, G., *"*Linear and nonlinear waves*." Wiley, New York*, 1974.

van De Sande B., Lansen, J., and Hoyng, C., "Sensitivity of coastal flood risk assessments to digital elevation models." *Water,* vol. 4, 568–579. doi: 10.3390/w4030568, 2012.

Vatvani, D., N. C. Zweers, M. V. Ormondt, A. J. Smale, H. D. Vries, and V. K. Makin, "Storm surge and wave simulations in the Gulf of Mexico using a consistent drag relation for atmospheric and storm surge models." *Natural Hazards and Earth System Sciences*, vol. 12(7), pp. 2399-2410, 2012.

Yoon, J. J., S. Shim, K. S. Park, and J. C. Lee, "Numerical experiments of storm winds, surges, and waves on the southern coast of Korea during Typhoon Sanba: the role of revising wind force." *Natural Hazards and Earth System Sciences*, vol. 14, pp. 3279–3295, 2014

Mei, C., "The applied dynamics of ocean surface waves." *Wiley, New York*. 1983.

VITA

Luca Castrucci was born in Anagni, Italy in 1994. After graduating from the scientific high school Francesco Severi of Frosinone, he moved to the United States of America and attended Old Dominion University in 2012. Four years later, following his graduating cum laude with a Bachelor of Science degree in Civil Engineering, he decided to join Dr. Navid Tahvildari's research team and began his graduate studies in Water Resources and Coastal Engineering. He plans to continue his study in hydrodynamic modeling with a PhD in the field of Civil Engineering.